Detecting coastal change along the North Sea coast from open-source satellite images

MSc Thesis Earth Surface and Water,
Coastal Dynamics and Fluvial Systems

Freya Fenwick
5711355

1st supervisor:
Dr. Timothy Price

2nd supervisor:
Prof Dr. Gerben Ruessink

Department of Physical Geography
Faculty of Geosciences
Utrecht University
The Netherlands

12 July 2021

Abstract

Sandy coastlines are continuously subjected to rapid coastal change. The expected climate change induced developments in sea level rise, mean wave conditions and storm events, will cause an increase in erosion rates, exposing these areas to increasing hazardous conditions. For coastal management purposes it is important to observe and quantify these changes. This is especially relevant around the North Sea as this is a low-lying area containing a variety of beach morphologies and orientations. However, it remains unknown how all the various beaches around the North Sea respond morphologically to the water and wave conditions in the North Sea. It is also unclear how these responses vary from one another and under what conditions these variations occur. Here we show that shoreline change around the North Sea is highly dependent on the site-specific circumstances and that storms are not the dominating factor determining the shoreline position. All studied sites exhibit long-term trends in shoreline position and morphological change. These trends show large variations between the different sites and are characterized by local factors such as morphology, orientation, local wave climate and coastal management strategies.

Table of Contents

List of Figures

List of Tables

1. Introduction

1.1 Background

Coastal areas are considered to be the most heavily urbanised areas in the world and are thus of great importance and economic value (Small et al., 2011). However, these areas are heavily affected by mean sea level rise, storm surges and other extreme wave events, which cause them to be vulnerable to rapid coastal change (Vos et al., 2019b). Also, the accelerated mean sea level rise due to climate change, has been seen as an important influence on coastal areas, causing for increasing erosion rates in coastal zones (De Winter et al., 2012; Field, 2014). It is thus very likely that these areas will be exposed to increasing hazardous conditions. Therefore, it is important for coastal management and development to observe and quantify these rapid alterations along susceptible areas of the coastline.

While understanding the evolvement of sandy coastlines requires comprehension of several morphological features, the position of the shoreline is generally considered as a key variable by coastal practitioners (Vos et al., 2019a). The location of the shoreline and the accompanying trends contain important information on coastal variations and are widely used in coastal zone management and policy making (Hagenaars et al., 2018).

Good coastal management along the North Sea coastal zone is especially relevant, as these areas are heavily populated and low-lying (De Winter et al., 2015), causing them to be extra vulnerable to the effects of climate change (Masselink et al., 2016). Morphological developments of long sandy coastal stretches, such as the Dutch North Sea coast, can vary hugely (Del Rio et al., 2013; Harley et al., 2017). Harley et al. (2017) state that different coastal orientations and varying weather, among other factors, can lead to local differences in morphological response.

The beaches surrounding the North Sea have a variety of orientations and morphological characterizations. However, it remains unknown how all these beaches respond morphologically to the water and wave conditions in the North Sea, and how these responses vary from one another. Also, it is unclear if these variations occur under regular conditions or only during storm conditions.

According to Boak and Turner (2005) there are two main categories of shoreline interpretations: those derived from aerial photographs or video imagery based on a visible dividing line (1), or otherwise a shoreline based on a common elevation datum, derived from in-situ measurements (2). In-situ data is often very accurate yet lacks spatial and temporal resolution as collecting this data is highly time and money consuming. However, publicly available satellite imagery provides vast amounts of data with a high spatial and temporal scale at low costs. Critical in this, is the arrival of Google Earth Engine (Gorelick et al., 2017), which offers access to a vast amount of publicly available satellite images that is continuously growing as well. The arrival of multi-decadal publicly available satellite images provides new opportunities for shoreline research over larger spatial and temporal scales as well as a variety of techniques (Liu et al., 2017; Luijendijk et al., 2018).

Recently, Vos et al. (2019b) introduced a new open-source software toolkit, CoastSat, which is designed to semi-automatically map shorelines from 30+ years of available satellite imagery with a horizontal accuracy of ~10 metres. This new toolkit allows for coastal monitoring free of charge on a seasonal to decadal time scale as well as with a high horizontal accuracy (Vos et al., 2019a). With this, CoastSat is an essential next step in the continuously evolving and growing technological evolution of satellite remote sensing and therefore coastal zone management.

This MSc thesis aims at improving understanding of shoreline behaviour at various spatial and temporal scales at contrasting sites around the North Sea, while also testing the applicability of CoastSat to these various sites around the North Sea.

1.2 Short-term shoreline variability

Sandy coastlines are highly variable, as their dynamics cover a large range of spatial and temporal scales (Stive et al., 2002). The various scales each have their own causes and effects for shoreline change, as well as inter scale relations.

On the shorter end of the temporal scale (i.e., individual storms and seasonal variability), shoreline change is dominated by cross-shore processes interfering with the local dynamics. These predominantly consist of sediment displacement induced by temporal variations in wave conditions (Splinter et al., 2014; Stive et al., 2002) as on this end of the spectrum, spatial shoreline change is controlled by variabilities in incoming wave energy (Davidson et al, 2013; Yates et al., 2009).

The response of sandy coastlines to incidental events (i.e., storms) is highly variable (Masselink et al., 2016; Scott et al., 2016), not only between different sites but also within a single coastal stretch (Haerens et al., 2012). Factors influencing storm response of coastal stretches include both internal and external components. The complexity of short-term shoreline response is enhanced due to the interaction between these internal and external factors. Furthermore, temporal variations in wave characteristics also occur on seasonal or annual time scales, causing for shoreline change on slightly longer timescales. One of these factors for instance, are the tidal spring-neap cycles. Specific examples of the complexity and variability of shoreline response on different spatial and temporal scales are given below.

Haerens et al. (2012) describe the various reactions of the entire Belgian coastal stretch over a timespan of 25 years. They found that for most storms only one to three areas of the ten distinguished areas in total, show some traces of the storms. External factors such as the alongshore variability of the storm processes and the geographical location of the site relative to the storm centre could be the cause of the morphologically various responses, but the wide span of morphological beach types along the Belgian coastline are another illustrative factor. These internal factors, such as the present morphology, beach slope, sediment size (Morton, 2002) are known to be important factors. Another factor causing the differentiated morphological response of the Belgian coastal stretch, is the various nearshore and offshore

sandbank morphologies. It was found that areas least affected by storm erosion are the most western areas along the Belgian coastline, which have the mildest slopes and large shallow near shore banks, which most likely have a dampening effect on the wave climate (Haerens et al., 2012).

A single beach can also show various reactions to almost similar storms. Harley et al. (2016) investigated the different responses of the Narrabeen-Callaroy beach to two different (but similar) storms eight years apart. They found that the slightly more severe storm of 2015, in terms of offshore wave conditions, caused less absolute erosion than the slightly less severe storm of 2007. They argue that the reasons for this inconsistency can be directly related to the available sand stored within the pre-storm berm, as the 2007 pre-storm berm consisted of significant larger sand volumes than the 2015 pre-storm berm. Furthermore, the specific areas with these larger beach volumes showed the largest erosion rates, whereas areas with near equal pre-storm berm volumes also showed similar erosion volumes during both storms.

When analysing the differentiated response of numerous sandy beaches to the same storm event or season, relations between beach exposure and erosion were found. Both Scott et al (2016) and Masselink et al. (2016) found that fully exposed sandy beaches are dominated by cross-shore sediment processes on a seasonal scale, transporting sediment from supra- or intertidal storages towards subtidal areas (nearshore bars) and thus are prone to severe beach erosion. In contrast, semi-sheltered sites with a more oblique wavefield are shown to be dominated by beach rotation (event/seasonal scale), due to alongshore sediment redistribution instead of sediment loss in the intertidal areas. Alongshore variabilities can thus also cause for cross-shore shoreline mobility. These alongshore variables are also commonly relevant on interannual or interdecadal timescales (Stive et al., 2002).

Moreover, alongshore variabilities in beach shape occur on different spatial scales, from tens to a thousand meters and from tens to hundreds of kilometres. Starting at the shorter end of the scale, variability in beach width can occur with striking rhythmicity on rip-channel beaches, caused by the presence of near shore crescentic sandbars *(Figure 1A)* or transverse bars *(Figure 1B)* (Aagaard,1988; Castelle et al., 2015; Winter, 2012).

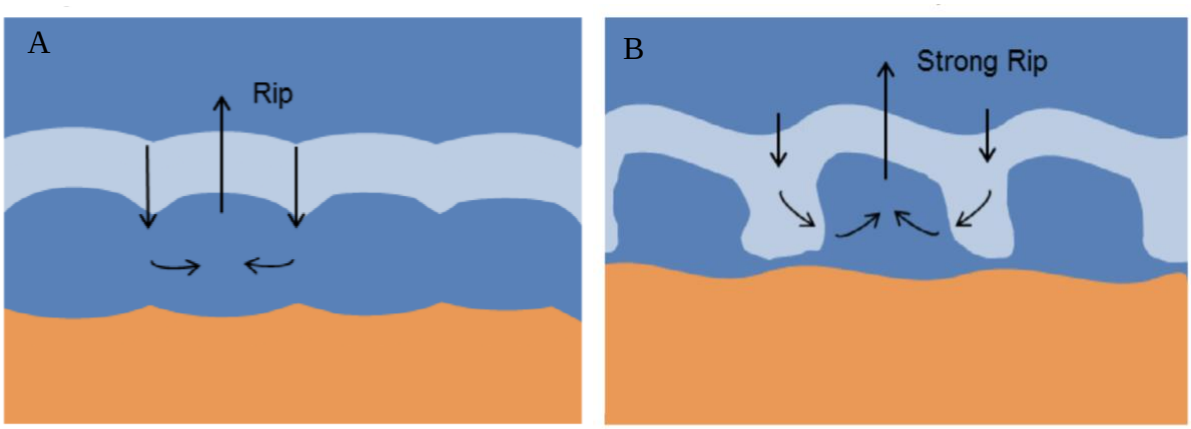

Figure 1. Rip-channel forming rhythmic shoreline patterns: (A) rhythmic bar and beach; (B) transverse bar and rip. Figure by Winter (2012).

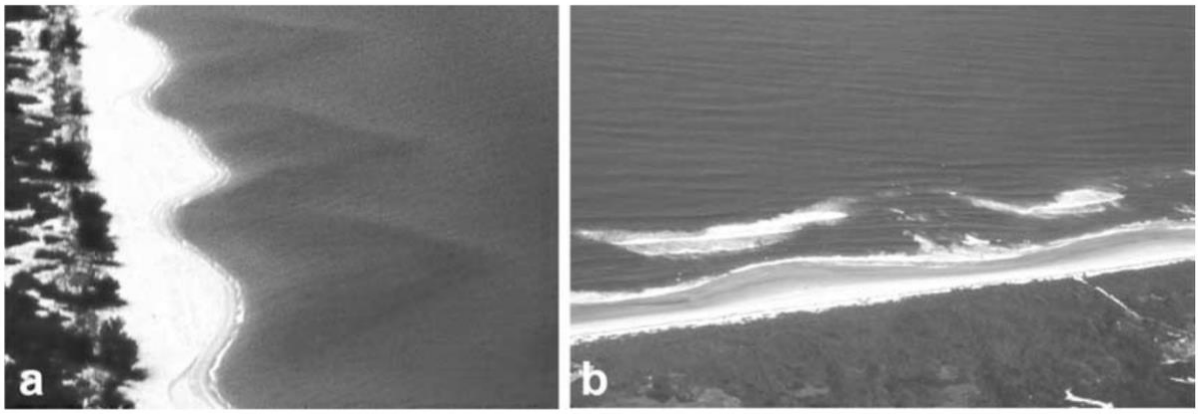

Figure 2. Aerial photographs of a single-barred beach of the New South Wales Coast (Australia) displaying (A) a 180° out-of-phase relationship of inner-bar patterns and shoreline rhythms with inner-bar bays systematically facing a seaward bulge in the shoreline and (B) an in-phase relationship between inner-bar patterns and shoreline rhythms (Figure and description adopted from Castelle et al., 2010).

Near shore sandbar morphology is often coupled to the shoreline and is another important factor contributing to shoreline change on timescales from days to months, though this is highly site specific (Ruessink et al., 2007; Price & Ruessink, 2013; Van de Lageweg et al., 2013). Both out-of-phase, shoreward-directed shoals face offshore shoreline perturbation *(Figure 2A)*, and in-phase, shoreward-directed shoals face onshore shoreline perturbations *(Figure 2B)*, relationships of inner-bar patterns and shoreline rhythms occur (Castelle et al., 2010). Rhythmic patterns, on larger temporal and spatial scales cause for increasing amounts of shoreline curvature and with this an increasing alongshore variability of the wave climate. Recent studies have shown how variabilities in the local wave climate have a possibly decisive effect on the morphological evolution of nearshore sandbars and in turn their effects on shorelines (Gijsman et al., 2021; Rutten et al., 2018, 2019).

An example of sandbar-shoreline coupling around the North Sea is given in Stive et al. (2002). The study shows that along a large coastal stretch of the Dutch Holland coast, certain cross-shore positions of the bar configurations favour offshore dissipation of wave energy and thus shoreline accretion, while other configurations promote beach and shoreline erosion. Typically, these bar positions show a return period between 10-15 years.

1.3 Long-term shoreline variability

Moving over to the longer end of shoreline change spectrum, multi-year and decadal shoreline change is mostly controlled by sediment budget (Castelle et al., 2018), including gradients in longshore sediment transport, variations in river sediment supply and sea level rise or fall (Pranzini and Williams, 2013). Shoreline change can extend onto geological timescales in the form of chronic accretion or erosion, due to sea level variations, which have happened many times before in the Earth's history (Regnauld et al., 1996). Le Cozannet et al. (2016), showed that shoreline change due to sea level variations can only be captured in a timeseries of at least fifty years, whereas shoreline evolution driven by other processes can be captured on shorter timeseries.

Mixed energy environments, such as tidal inlets and estuary mouths, lead to increasingly complicated shoreline dynamics as these areas are extremely susceptible to change (Castelle et al., 2007). Cyclic behaviour in such tidal environments is very common and has typical timescales varying from months to years or decades (Castelle et al., 2018; Ridderinkhof et al., 2016a, Ridderinkhof 2016b). Typical for ebb-tidal deltas is the growth and updrift or downdrift migration of sandy shoals, which often leads to large morphological and sedimentary disturbances of the updrift/downdrift coasts as the attachment of a shoal could supply the coast with vast amounts of sand (10^6 m^3) (Hofstede, 1999) (Ridderinkhof et al., 2016a). Such cyclic behaviour can lead to cyclic shoreline change of adjacent, downdrift or updrift shorelines (Castelle et al., 2007).

A clear example of this is the periodic sediment supply from the ebb-tidal deltas in the North Sea to the downdrift Wadden islands, causing the coastline to be highly fluctuating on a yearly and decadal timescale (Wang et al., 2012). Due to periodic onshore migration of ebb-tidal deltas, Schiermonnikoog has a periodic fluctuating mean low tide line (MLT) which, after a time lag and with a lower amplitude, the average coastline and dune foot position follow. The typical duration of the periodic fluctuations here is between 20 to 30 years and is accompanied by a seaward migrating trend of the coastline (Prakken, 1989).

Another example of cyclic shoal behaviour in the North Sea, is the shoal attachment downdrift of the Accumer Ee to the coast of Langeoog barrier island, located just 75 km northwest of Schiermonnikoog. A total of ten shoals migrated towards Langeoog between 1984-1990 and 1998-2014 (*Figure 3*) of which some merged before becoming attached to the barrier island (Ridderinkhof, 2016b). The shoal behaviour on the ebb-tidal delta of the Accumer Ee has a

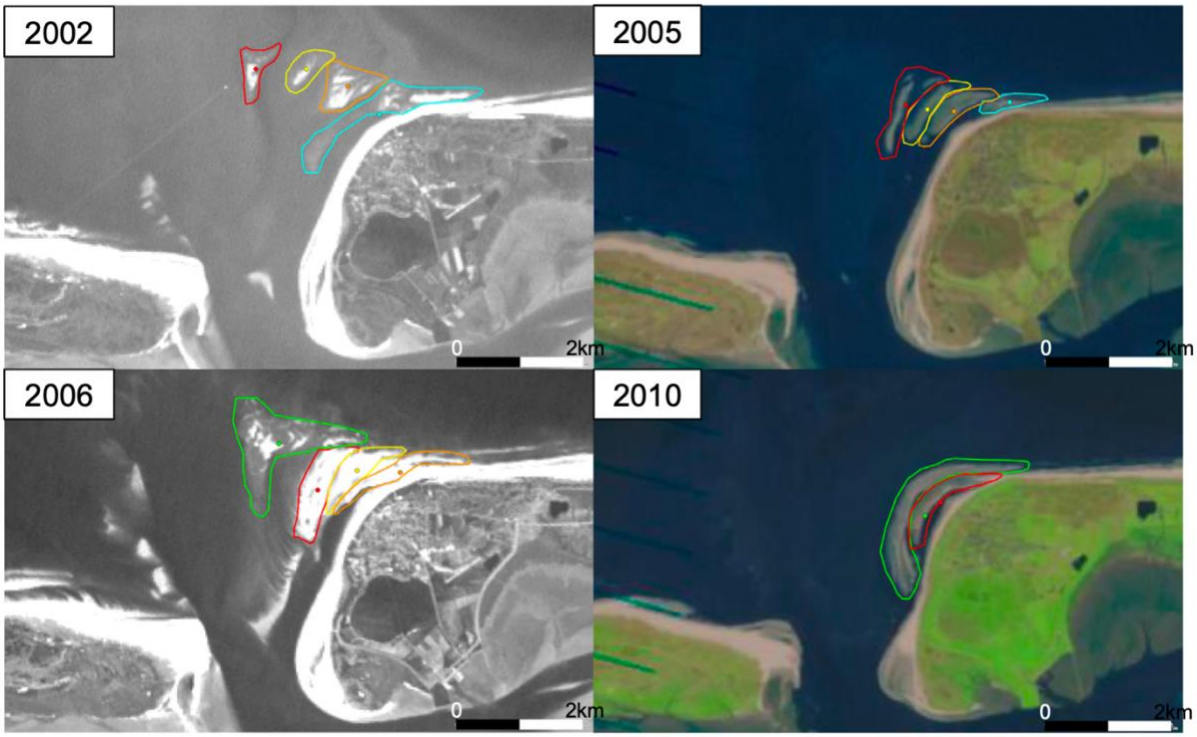

Figure 3. Landsat satellite images of the attachment of several shoals from the ebb-tidal delta to the barrier island of Langeoog from 2002 to 2010. Image from Ridderinkhof (2016b).

high morphodynamics activity compared to the other ebb-tidal deltas in the area. As can be seen on the satellite images in *Figure 3*, the shape of the shoals is seen to distort closer towards the shoal as they bend around the island head. Ridderinkhof (2016b) state that the merging and distortion of the shoals is due to the fact that the migration velocity of the shoals often decreases when the shoals get closer to the coast.

1.4 Human-induced shoreline variability

In addition to all previously mentioned natural causes for shoreline variations, human-induced interference in coastal zones cannot be excluded. Hard structures, such as groynes and dikes have been used successfully in the past to protect the hinterland from flooding, nonetheless they hugely influence local sediment transport and often are the cause for adverse effects (Firth et al., 2014). Further up the sediment supply chain, river damming is known to have a significant reducing effect on sediment supply to coastal areas (Nienhuis & van de Wal, 2021).

Anthropogenic influences in the coastal zone have almost entirely switched from predominantly building hard structures to soft structures referred to as 'Building with Nature' (Stronkhorst et al., 2018). These include sand nourishments, which can be placed in the shoreface *(Figure 4A)*, on the beach or dune face *(Figure 4B)*, and provide numerous ecosystem services, next to coastal defence (De Vriend et al., 2015). The expected effect of the shoreface nourishments is built up on the lee and feeder effect to increase the volume of sediment shoreward of the nourishments (Ojeda et al., 2008) The lee effect is explained as the ability to increase wave dissipation on the nourishment, resulting in a calmer wave climate behind the nourishment and a decreased alongshore current (*Figure 5A)*. The feeder effect is the onshore transportation of sand from the nourishment by wave non-linearity and onshore currents, eventually resulting in the onshore migration of the nourishment (*Figure 5B)* (Grunnet & Ruessink, 2005; van Duin et al., 2004). As *Figure 5* illustrates for shoreface nourishments, the influence of soft and hard engineering structures is known to reach beyond the local area and can affect shorelines further alongshore from the nourishment (De Schipper et al., 2016; Huisman et al., 2019).

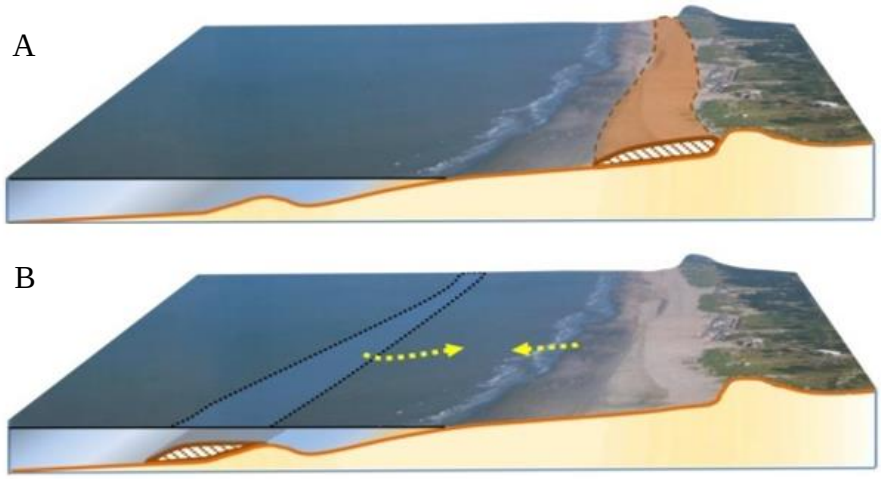

Figure 4. Different sand nourishment types: (A) beach or dune face nourishments; (B) shoreface nourishments. Figure by de Schipper (2014).

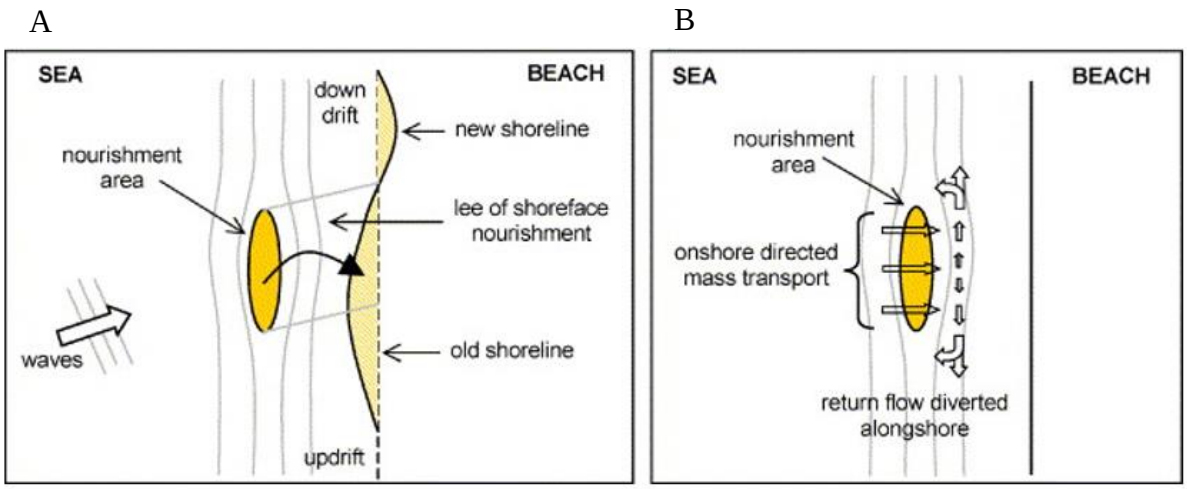

Figure 5. Effect of shoreface nourishment: (A) lee effect; (B) feeder effect. Figure by van Duin et al. (2014).

1.5 Research Questions

Sandy coastlines are extremely susceptible to coastal change and the highly populated, low lying areas along the North Sea coastal zone need to be managed accordingly to be able to adapt to the expected climate induced changes. For proper management, more insight on shoreline behaviour is needed as well as a better understanding of the conditions causing these changes. Specifically, in this thesis the focus is put on previously described local 'internal' factors.

This MSc thesis has two main objectives. The first objective is to assess the applicability of CoastSat on the North Sea coasts. The second objective is to compare the shoreline behaviour at contrasting sites around the North Sea. These objectives will be attained by answering the following research questions:

1. How does the applicability of CoastSat vary between different North Sea coastal areas?
    a. What is the influence of the various tidal ranges around the North Sea?
    b. What is the influence of differences in morphology or various beach characteristics?
2. How have the shorelines around the North Sea evolved during the last few decades?
    a. What are the natural trends (e.g., seasonal, annual, or perennial) of the shorelines of the different beaches around the North Sea?
    b. How do the various shorelines respond to storm conditions?
    c. How do these natural trends and storm responses vary at a single site, or compared between sites?
    d. What wave conditions (e.g., wind- and wave direction, period, and speed) stimulate shoreline variations along the various coastal areas?

This thesis will start off with a description of the different study sites (Chapter 2), followed by a detailed explanation of all collected data and methods used to obtain, process, and analyse our results (Chapter 3), which will then be presented in Chapter 4. These results will then be analysed and compared between the different study sites and known literature as in Chapter 5. Final conclusions will then be drawn and presented in the final chapter of this thesis (Chapter 6).

2. Study Site Description

2.1 North Sea Basin

The North Sea is a semi-enclosed shallow basin, consisting of the area south of 62° N, the English Channel, and the Scandinavian Straits (NSTF, 1993). Its eastern coasts are predominantly sand beaches with dunes, whereas it's northern and western coasts contain a variety of shore types (e.g., estuaries, fjords, rocky shores, and cliffs) (Nienhuis, 1996).

Winds are seasonal with high winds in spring, the main wind direction is Western with alternating easterly winds. However due to the shape of the basin and the long fetch, the strongest winds are North-western (Ducrotoy et al 2000). Tides are semi-diurnal and sinusoidal (Hardisty 1990; Pugh, 1987). Along the Dutch coast the tidal range decreases from 3 to 1.25 meters, and then increases again towards the Wadden Sea. As the seasonal fluctuations in hydrometeorological conditions are large along the North Sea, the beaches are considered storm dominated, increasing towards the South (Ducrotoy et al., 2000; Winkelmolen & Veenstra, 1980).

For the shoreline change analyses five long sandy beaches around the North Sea were selected: (1) Egmond aan Zee and (2) the barrier island of Schiermonnikoog, both in the Netherlands, (3) Skallingen in Denmark, (4) Groenendijk in Belgium, and (5) Theddlethorpe in the United Kingdom *(Figure 6).* All have varying tidal ranges, orientations, and wave exposure.

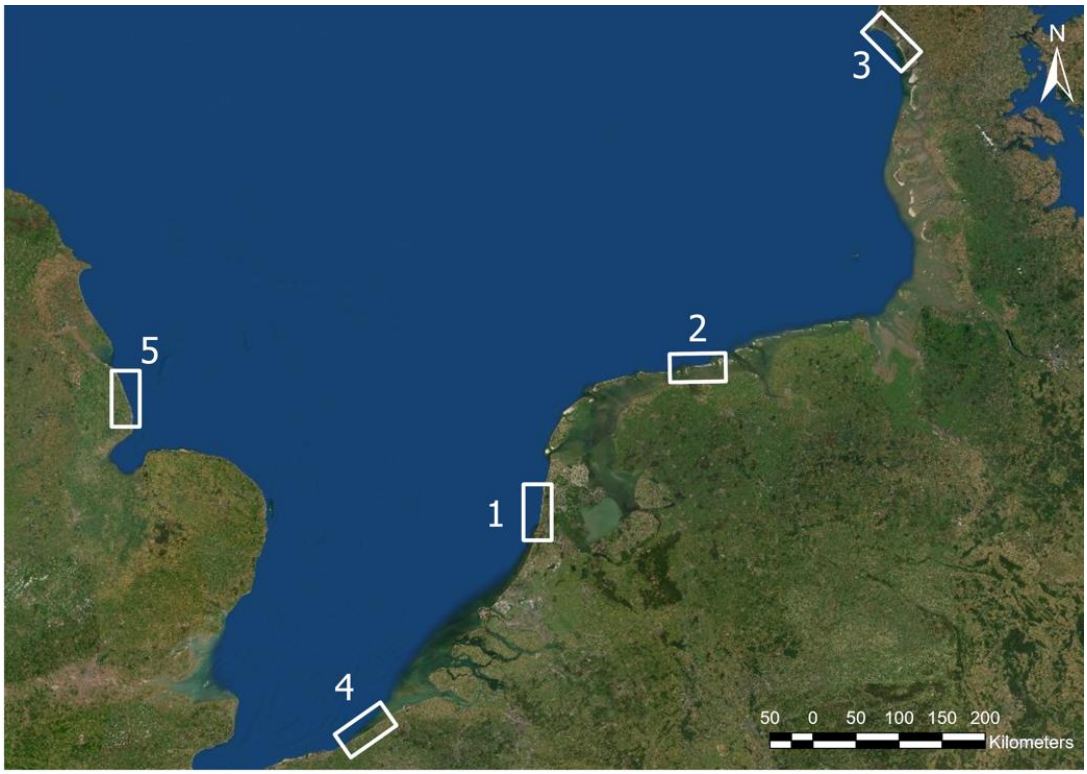

Figure 6. Overview of the North Sea basin with the location and orientations of the five study sites: (1) Egmond aan Zee, NL; (2) Schiermonnikoog NL; (3) Skallingen, DK; (4) Groenendijk, BE; (5) Theddlethorpe, UK (5).

2.2 Netherlands

The Dutch North Sea coast is 432 kilometre long, of which 254 kilometre is fringed by sandy areas or dunes. The Dutch coast can be divided into three morphologically very distinguishable areas: The Delta Coast in the South, the central Holland Coast, and the Wadden Coast in the North (Ruessink & Jeuken, 2002). A study site in each of the two latter named areas is analysed, Egmond aan Zee and Schiermonnikoog respectively, and will be discussed in further detail.

2.2.1 Egmond aan Zee

The central Holland Coast is a sandy, uninterrupted, slightly curved, NNE-SSW orientated, 120-kilometre-long coastline which faces the North Sea. This long coastal stretch is bordered by a tidal inlet to the North (Marsdiep), and the outflow of the river Rhine, which is connected to the Harbour of Rotterdam, to the South. The Rhine outlet has 3-kilometre-long jetties, making this Southern border a hard structure (Wijnberg, 2002).

Along the central Holland Coast there are shoreface-connected ridges, sandbars, situated at water depths between 14-18 metres. These sandy bars are 2-4 kilometres wide and up to 30 kilometres long, with a height varying between 2-6 metres (van de Meene & van Rijn, 2000).

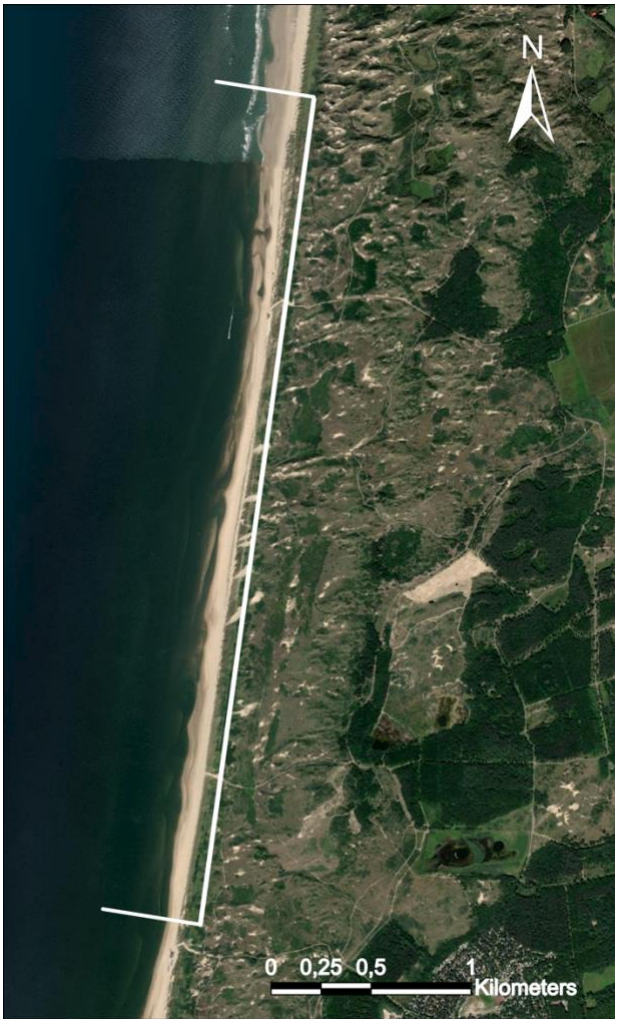

Figure 7. Satellite image of the first study site Egmond aan Zee in the Netherlands, showing the local near shore morphology. The shoreline has a SSW-NNE orientation and borders the North Sea to the west. The specific study area is indicated between the white lines and has an alongshore width of approximately 4000 meters.

Egmond aan Zee is situated along this central Holland Coast *(Figure 7)*. The site is high-wave storm-dominated and is considered micro- to meso-tidal, with the tidal range varying between 1.65 and 2.1 metres for neap and spring tide, respectively. The tide is semi-diurnal and asymmetric, with a 4-hour flood period and 8-hour ebb period (Aagaard et al., 2005).

The annual mean offshore wave height is 1.2 metres with an average wave period of 5.0 seconds (Van Rijn et al., 2002). The most frequent winds are from the southwest, but the real storm surges only occur with strong winds from the northwest, which can raise the water level by more than 1 metre (Ruessink et al., 2019). The shoreface is gently sloping (~1:40) and has an intertidal zone of around 50-100 metres wide, classically including semi-rhythmic intertidal bars and rip channels (Aagaard et al., 2005). The beach becomes steeper above the high-tide level and steeper again as it leads up to the front face of the foredune, with the foredune crest located between 20-25 metres +MSL (Ruessink et al., 2019). Locally, the sand consists of well sorted grains with a median size of 250-300 μm and a landward fining trend up to 200 μm (Aagaard et al., 2005; Ruessink et al., 2019). The coastal area right in front of the town Egmond aan Zee, just North of our research area, has been subject to frequent nourishments from 1990 up until the present. The nourishments have alternately been placed in the shoreface or on the beach (van Duin et al., 2004).

The nearshore zone consists of two subtidal sandbars, which are characteristically steep at Egmond with the bar crest being situated at 1.5-2 metres water depth and have deep intervening troughs (Aagaard et al., 2005). Generally, the inner bar has a crescentic appearance (Van Rijn et al., 2002). The beach state is intermediate, with alternating bars and horns having a more dissipative nature and intervening rip embayments which are more reflective of nature.

2.2.2 Schiermonnikoog

The Dutch Wadden Coast forms the Northern most part of the Netherlands and consist of a string of barrier islands, each separated by tidal inlets and tidal deltas. The islands have an ENE-WSW orientation, and their heads point in SSW-SW direction. These characteristic sandy island heads lack well-developed dunes, and form extensive beach planes (Prakken, 1989). In general, the parts that eroded during storms, recover wholly or partially due to accretion in calm conditions (Wang et al., 2012). In this part of the North Sea the tidal currents run parallel to the coast, towards the northeast during flood and during ebb towards the southwest (Sha, 1989b). Furthermore, wind-driven waves along the islands are most frequently from the SW-W (Sha, 1989b).

Schiermonnikoog is the most north-eastern situated island in the Dutch North Sea *(Figure 8)*. The beaches mainly face the North Sea and are characterized by being wide and flat (~1:60) (Vanagt et al., 2011). The supratidal zone along the coastline is several hundred metres wide, making room for primary dune fields which are significant for the extensive dune system on the barrier island (Bakker er al., 2005).

Figure 8. Satellite image of the second study site Schiermonnikoog in the Netherlands, showing the local near shore morphology. The shoreline has a WSW-ENE orientation and borders the North Sea to the North. The specific study area is indicated between the white lines and has an alongshore width of approximately 14000 meters.

The area is categorized as mesotidal, with a spring tidal range of 2.2 metres (Hesp & Arens, 1997; Postma 1982). The sand is very well sorted and reasonably fine as the mean grain size is 170 μm (Arens, 1994). During calm conditions the wave height is around 1 metre (MeteoBlue, 2020), with a mean significant offshore wave height of 1.18 and a peak period of 5.77 seconds (Ridderinkhof et al., 2016b). Schiermonnikoog is the only Dutch Wadden Island that has not been subject to sand nourishments.

2.3 Skallingen, DK

The Danish North Sea coast occupies almost the entire western part of Jutland *(Figure 6)*, the exception being the Wadden Sea coast in the southernmost area. This North Sea faced, west coast consists mainly of barrier beaches and sandy coastal stretches (Pranzini & Williams, 2013). These barriers are often protected by urban development or ports, with only a few areas left untouched by human interference (Aagaard et al., 2004b).

The barrier of Skallingen is situated in the southwestern part of the Danish North Sea coast *(Figure 9)*. The coastline has an almost exact NW-SE orientation. The barrier has an 80-100 metres wide beach, which includes the intertidal zone and the foredune zone (Aagaard et al., 2004a). The barrier has undergone some anthropogenic alterations for coastal protection. These include an area of groynes at the Northern end and two groynes at the southern point of the barrier. The section between these barriers has been left to its natural state, without any large anthropogenic influences (Aagaard et al., 2004b).

The subtidal beach is extremely low sloping (1:200), whereas the intertidal zone has a slightly steeper slope (~1:30-1:50). The lower shoreface consists of some minor bar relief. There are 2-3 subtidal bars in addition to a highly mobile intertidal bar (Aagaard, 2002). The outer bars are more longshore uniform, whereas the nearshore and intertidal bar are more commonly dissected by rip channels (Aagaard et al., 2004a).

Figure 9. Satellite image of the third study site Skallingen in Denmark, showing the l.ocal near shore morphology. The shoreline has a NW-SE orientation and borders the North Sea to the Southwest. The specific study area is indicated between the white lines and has an alongshore width of approximately 9000 meters.

In the lower shoreface the sand is quite fine as median grain size is 110-120 μm. This increases in shoreward direction up to 150-200 μm (Aagaard., 2002), causing an opposite trend from the onshore fining trend found at Egmond.

Skallingen is subject to the high wind and wave climate of the North Sea and is heavily impacted by storm surges. The mean annual offshore wave height is 1.0 metres, which can exceed 5 metres during storm events. The wave periods are between 4-6 and 10-13 seconds during calm conditions and storm events respectively. The site is considered microtidal and is subject to a semi-diurnal tide. The mean tidal range is 1.5 metres, which can increase up to 1.8 metres during spring tide (Aagaard et al., 2004a). The area is dominated by a wind and wave field from the W-NW (Pranzini & Williams, 2013), although the high storm surges occur when winds originate from the Southwest and west southwest (Christiansen et al., 2004).

2.4 Groenendijk, BE

The Belgian North Sea coastline is approximately 65 kilometres long and is part of the sandy southern North Sea coastline (*Haerens et al., 2012)*. The coastline is considered macrotidal, with a tidal range varying between 3.5 and 5.0 metres for neap and spring tide, respectively (Short, 1991). The semi-diurnal tide has a small asymmetry (Haerens et al., 2012). The coast has a SW-NE orientation (55-235°), which results in a longshore drift toward the northeast (Brand et al., 2020). There are numerous sand banks present along the coast, which are in the range of tens of kilometres long and a few kilometres wide (Van Oyen et al., 2013). The orientation of these banks is generally WSW-ENE and are thus roughly parallel or sub-parallel to the coastline (Anthony, 2013). The beach slopes increase from west (1:75) to east (1:40),

Figure 10. Satellite image of the fourth study site Groenendijk in Belgium, showing the local near shore morphology. The shoreline has a SW-NE orientation and borders the North Sea to the Northwest. The specific study area is indicated between the white lines and has an alongshore width of approximately 3000 meters.

which results in a narrowing of the intertidal beach width in this same direction; 500-600 metres in the west in Panne to 200-300 metres in the east in Knokke (Deronde et al., 2006).

The average wave height is 0.5-1 metres, and the average wave period is 3.5-4.5 seconds. Offshore waves are mainly driven by westerly winds (WSW-NW) (Van Lancker, 1999) and during storm surges, southwest, west or northwest directions prevail (Haerens et al., 2012). The nearshore sand bank morphology, in conjunction with tidal modulation, may result in a highly variable wave field close to the beach (Héquette et al., 2009).

The Belgian coastal morphology has been highly influenced by the formation and migration of tidal inlets and interference with natural processes by anthropogenic factors (Pranzini & Williams, 2013). The tidal inlets are believed to be the largest sediment sinks and are responsible for coastal erosion, but also cause accretion elsewhere along the shoreline (De Moor et al., 2010).

Anthropogenic factors include the building of hard protective structures and at a later stage changing to periodic beach nourishments. There is a small coastal stretch at Groenendijk, between the towns of Panne and Nieuwpoort which has had no anthropogenic interference (Pranzini & Williams, 2013) and this is our research area *(Figure 10)*.

Groenendijk is a natural beach near Nieuwpoort where no protected measures have been taken. The intertidal beach is gently sloping (1:100) (Brand et al., 2020), consists of four bars, making the width a total of 290 metres which is bordered by a ribbon of dunes of moderate (~20 metres)

height (De Moor et al., 2010). In general, the dunes along the Flemish coast have a height ranging between +5 and +30 metres TAW. TAW is the local Belgian height datum situated close to LAW (Lowest Astronomical Tide) and is situated 2.33 metres below the Dutch ordinance datum NAP (Haerens et al., 2012). The beach sediments have a median grain size of 200 μm (Brand et al., 2020).

2.5 Theddlethorpe, UK

On the Eastern Seaboard of the United Kingdom, Lincolnshire borders the western part of the North Sea between the Humber estuary and the Wash (Maselink & Anthony, 2001) *(Figure 6)*. The Northern section, from Donna Nook to Mablethorpe, consists of a 20-kilometre-long coastal stretch, belonging to the Humber estuary's ebb tidal delta. To the southern end of this area a sandy beach, devoid of any coastal engineering structures, is situated (Kroon & Masselink, 2002). This area called Theddlethorpe beach is our final research area *(Figure 11)*.

Figure 11. Satellite image of the fourth study site Theddlethorpe in the United Kingdom, showing the local near shore morphology. The shoreline has a NNW-SSE orientation and borders the North Sea to the East. The specific study area is indicated between the white lines and has an alongshore width of approximately 4500 meters.

Theddlethorpe beach begins just south of the Humber estuaries tidal inlet, is orientated in NNW-SSE direction, and has a width of approximately 400 metres, after which it is backed by dunes. The intertidal area is characterised by several well-developed intertidal bar systems and generally has a gentle slope (varying between 1:60 – 1:100) decreasing towards the North (Van Houwelingen et al., 2006). A couple of kilometres to the south this wide beach disappears, and the intertidal area is directly bordered by the dune field (Kroon & Masselink, 2002). The sediment in this area shows a very distinct break in sand particle sizes around MSL. Above this datum, the D_{50} is slightly coarser and varies between 180-210 μm, whereas below MSL, it varies between 160 and 180 μm (Masselink & Anthony, 2001). The sediment thus shows an offshore fining trend similar to observations at Skallingen.
The area is considered macrotidal, with a mean spring tidal range of 6 metres. The tide is semidiurnal, with flood currents directed to the south and ebb currents to the north (Kroon & Masselink, 2002). The main wind direction is from the southwest. However, during the winter months these winds change direction and become north-westerly and easterly winds, causing the predominant wind direction in this area to be offshore (Masselink & Anthony, 2001). The significant wave height varied between 0.1-0.4 metres with accompanying wave periods of 4-7 seconds (Kroon & Masselink, 2002).

2.6 Summary

As all study sites have varying orientations, beach widths, slopes, tidal ranges etc., an overview of the site-specific characteristics is given in *Table 1* as a summary.

	Egmond aan Zee	**Schiermonnikoog**	**Skallingen**	**Groenendijk**	**Theddlethorpe**
Orientation	NNE-SSW	ENE-WSW	NW-SE	SW-NE	NNW-SSE
Beach length (m)	4000	14000	9500	3000	4500
Width intertidal area (m)	50 - 100	≥200	90	290	300
Slope	~1:40	~1:60	~1:40	~1:100	~1:80
Tidal range (m)	≤2.1	≤2.2	≤1.8	≤5.0	≤6
Average wave height (m)	1.2	1.2	1.0	0.5 – 1.0	0.1 – 0.4
Average wave period (s)	5.0	5.5	4 – 6	3.5 – 4.5	4 – 7
D50 (μm)	200 – 300	170	110 - 200	200	160 – 180

Table 1. An overview of the site-specific characteristics per study site.

3. Methodology and Data Description

This research uses several different toolkits and programs for the shoreline analyses. The main toolkit is a new open-source available automated shoreline detection program CoastSat (Vos et al., 2019b), which algorithm and techniques are discussed in detail in Section 3.1, whereas the specific use of CoastSat for this research is described in Section 3.2. Furthermore, the collected datasets required for this thesis and the tools and -techniques used for further analyses is described in Section 3.3.

3.1 CoastSat

CoastSat is an open-source Python software toolkit created by Kilian Vos (Vos et al., 2019b). It is designed to map shorelines from publicly available satellite imagery. The satellite images are retrieved from Google Earth Engine (GEE) (Gorelick et al., 2017), which allows the user to obtain more than 30 years of shoreline data.

It should be noted that CoastSat works for any sandy beach over the world and obtains shorelines with a horizontal accuracy of ~10 meters. When comparing this with previous shoreline detection algorithms, such as Hagenaars et al. (2018), CoastSat has a significant enhancement of the spatial resolution. A sub-pixel shoreline extraction has led to the accuracy of the satellite derived shorelines, no longer being limited to the spatial resolution of the pixel size of the satellites (Vos et al., 2019a).

CoastSat uses a number of freely available toolkits, which are combined and extended into a single toolkit. The functionality of CoastSat can be summarised as several sequential steps provided within the toolkit (Vos et al., 2019b):

i. Retrieval of the images from the GEE archive;
ii. Pre-processing of the multispectral images (cloud masking, pan-sharpening and down-sampling);
iii. Sub-pixel resolution shoreline extraction;
iv. Time-series of shoreline position along shore normal transects; and
v. Tidal correction of the time-series of shoreline position along shore normal transects.

A more detailed explanation of these different steps and techniques is given in the following sections.

3.1.1. Available satellite imagery and pre-processing

The toolkit provides access to GEE from which Top-of-Atmosphere (TOA) reflectance images are downloaded from Landsat 5 (TM), Landsat 7 (EMT+) and Landsat 8 (OLI) Tier 1 in addition to Sentinel-2 (MSI) Level-1C satellite images. This TOA reflectance creates a standardised comparison between images required from different sensors at different dates with different weather conditions (Chander et al., 2009). To decrease the size of the requested files, the user defines a region of interest (ROI) in advance, which is used to crop the images before they are downloaded. Also, only the spectral bands required for the shoreline detection (R, G, B, NIR and SWIR1) are included in the cropped image. These two adjustments significantly decrease the file size and increase the processing speed so that the tool can be used more

widely. The now cropped image is pre-processed so that the shoreline can be defined on a sub-pixel resolution and the interface between sand/water is created automatically (Vos et al., 2019b).

For pre-processing purposes an additional quality assessment band is downloaded. This band includes a per-pixel cloud mask, which is used to determine the percentage of cloud cover in the user defined ROI (Vos et al., 2019a). The user can define a cloud threshold to discard all images exceeding this cloud cover percentage. To enhance the shoreline detection a final pre-processing step is applied in the form of panchromatic image sharpening and down-sampling (Vos et al., 2019a).

3.1.2 Shoreline Extraction

The shoreline obtained by CoastSat is defined as "the instantaneous interface between water and sand captured at the instant of image acquisition" (Vos et al., 2019b, p.3). The toolkit contains a robust and generic algorithm to automatically extract the shoreline at subpixel resolution. The algorithm comprises three steps (Vos et al., 2019a): (1) image classification, (2) sub-pixel resolution border segmentation, and (3) tidal correction, which will be explained in further detail. In addition, the toolkit provides the option for the user to manually draw a reference shoreline, to help circumvent outliers or incorrect classifications.

Image Classification

To correctly determine the interface between sand and water, CoastSat contains a pre-trained classifier, which is used to label individual pixels to one of four classes: 'sand', 'water', 'white-water' and 'other land features' (e.g., vegetation building, rocky headlands). The classifier was trained manually during the study by Vos et al (2019a), with each class containing a set of 5000 pixels, taken from 50 satellite images covering 5 different sites. In the same study, the accuracy of the classifier was tested with a 10-fold cross-validation, resulting in an accuracy of 99%.

Sub-pixel Resolution Border Segmentation

A second step in the shoreline extraction is detecting the sub-pixel boundary between sand and water, by applying the Modified Normalized Difference Water Index (MNDWI) (Xu, 2006) to every classified image. The MNDWI is calculated as follows:

$$MNDWI = \frac{SWIR1 - Green}{SWIR1 + Green} \quad (1)$$

in which SWIR1 and Green are the pixel intensity in the short-wave infrared and green band, respectively (Vos et al., 2019a). The MNDWI value is computed for each pixel with values ranging between -1 and 1, which results in a single colour band image (Vos et al., 2019a). Subsequently, a histogram of MNDWI values is computed, which shows the probability density function (PDF) of each MNDWI value for the four different classes. To maximise the inter-class variance, the classes 'white-water' and 'other land features' are ignored while computing Otsu's threshold (Otsu, 1979) between the 'water' and 'sand' classes. This method provides a more stable boundary as the classes that do not contribute to identifying the

sand/water interface are not considered (Vos et al., 2019b). The final step of the shoreline extraction is a sub-pixel contouring algorithm. For further information concerning the individual toolkits and algorithms, please see Vos et al. (2019a).

Tidal Correction

As satellite images are required at any time, during any stage of the tidal cycle, single shorelines must be corrected for the tidal water levels, to allow for comparison and a correct time-series of shoreline positions. This is especially essential in areas with large tidal ranges, which our research areas have. To achieve the final cross-shore position of the satellite derived shorelines a simple horizontal translation, assuming a linear intertidal beach slope, must be implemented. This is done with the following correction:

$$\Delta x = \frac{Z_{ref} - Z_{wl}}{m} \quad (2)$$

which relocates each shoreline in the cross-shore direction (Δx) to a reference elevation (Z_{ref}), with the help of the local water level (Z_{wl}) and the characteristic beach face slope (Vos et al., 2019b). As a final step, the satellite derived shorelines are intersected with cross-shore transects along which the tidal correction (Δx) is applied. For this study, these transects were created using an ArcGIS function called 'Generate Transects Along Lines' (ArcGIS, 2021). The function plots evenly spaced transects, perpendicular to the shoreline *(Figure 12)*. Transects were spaced 50 metres apart throughout all study sites.

Figure 12. Shoreline perpendicular transects in white) along which the lateral tidal correction of the shoreline is performed.

3.2 Application of CoastSat

To acquire a proper understanding of the long-term shoreline behaviour around the North Sea, it is desirable for the timespan of our analyses to be as long as possible. Therefore, the begin point of our analyses coincided with the earliest available satellite images in GEE, which is 1984 (Gorelick et al., 2017) and is conducted up until 2020, comprising a timespan of 37 years. The second objective for our analyses, is obtaining a high temporal resolution. Therefore, all available and qualified satellite images were be used for this analysis. However, the number of images that qualify for the research is dependent on the coverage of the different satellites, local circumstances such as cloud cover and other restrictions that must be considered.

Firstly, only images from Landsat 5 (1984 - 2012), Landsat 8 (2013 - present) and Sentinel-2 (2015 - present) were used. Landsat 7 (2000 - present) was excluded from the research, due to a failing Scan Line Corrector (SLC) which caused all images acquired after May 31, 2003, to contain significant data gaps (United States Geological Survey (USGS), 2021). Moreover, the cloud cover threshold was set to 0.5, meaning that all satellite images with a cloud cover exceeding 50% were automatically discarded.

Throughout the usage of CoastSat, the user is provided with a number of options. One of them is to shows each shoreline to the user, giving the user the option to manually accept or reject the identified shorelines. This option was enabled, as correct shoreline detection can be obstructed by clouds or other interreferences *(Figure 13)*.

Another option the user has, is to manually adjust the position of the shoreline using the histogram of the MNDWI probability density function to adjust the land-water threshold *(Figure 14)*.

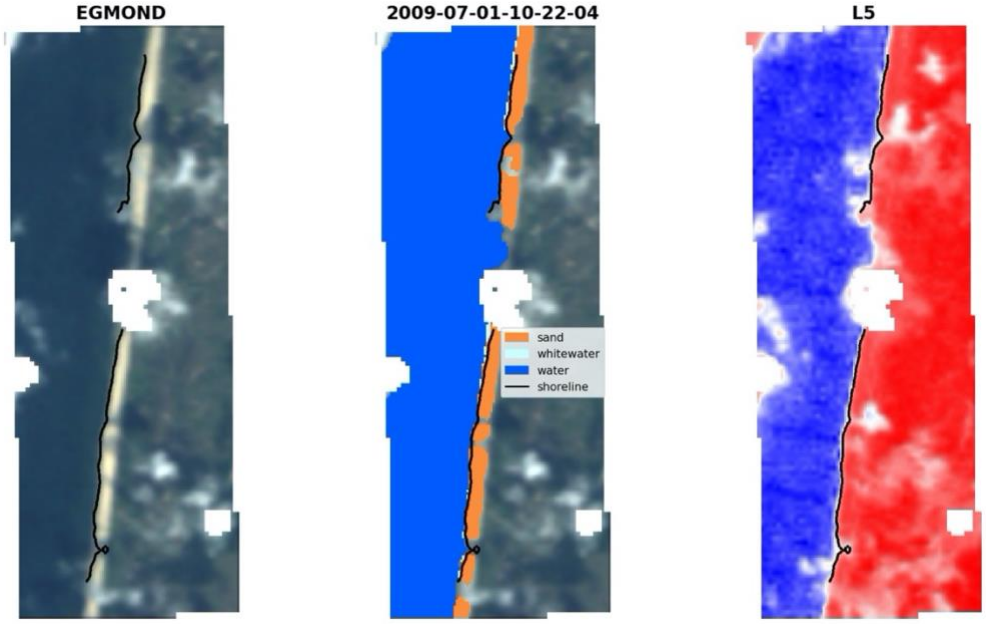

Figure 13. Example of a rejected shoreline for Egmond aan Zee. Cloudy weather hinders the algorithm and causes for an incorrect shoreline detection. The algorithm is programmed to delete large areas with cloudy pixels from the image as these closely resemble sandy pixels and can cause for incorrect classification. In this image however, not all clouds were detected, and the remaining pixels cause for an incorrect shoreline detection.

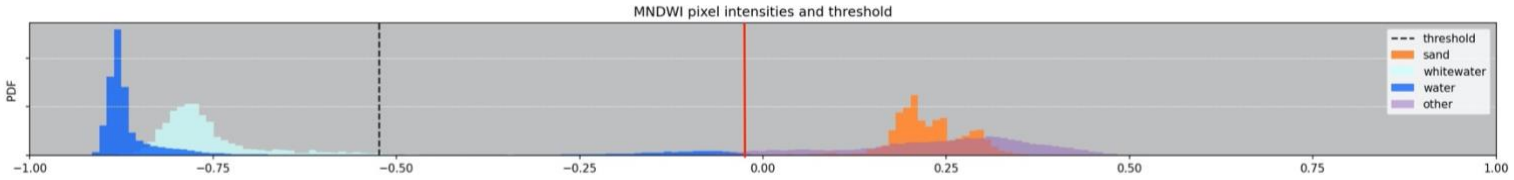

Figure 14. Histogram of MNDWI probability density function, indicating the pixel intensities and shoreline threshold. The red line indicates the automatically detected threshold, which was manually changed to the black threshold. The accompanying image can be found in Figure 15.

Starting the analyses, this function was turned off, as trained classifications and shoreline detection algorithms are seen as more accurate than human detection, as this is limited to eyesight. However, the automated shoreline detection caused for large fluctuations and sometimes even incorrect shoreline positions due to numerous reasons.

First, the algorithm seems to struggle with the difference between wet sand and water, which can lead to incorrect classification of the land-water interface. To demonstrate this, we will use Groenendijk as an example. Here we have a low sloping intertidal beach (1:100) with numerous sand banks located right in front of the beach *(Figure 10)*, where an outgoing tide almost instantly causes the shoreline to move tens to hundreds of metres seaward due to the low slope. This leaves large areas of wet sand, which is recognised by the algorithm as water *(Figure 15,* middle image). This means the land-water interface that is obtained automatically from the toolkit is in fact the boundary between wet and dry sand. The red line in the middle image of *Figure 15* shows the shoreline which was automatically detected by the algorithm. This initial shoreline being located incorrectly, also causes the tidal correction to be rather useless as the starting point of the correction is incorrect.
To solve this problem the threshold value of the MNDWI histogram *(Figure 14)* must be moved manually, to coincide with the real shoreline. Finding the correct position of the shoreline was mainly done based on the MNDWI image (*Figure 15*, right-handed image). The location where the MNDWI image shows a bright white signal, is the correct location of the sand-water interface. Also, when taking a closer look at the histogram in *Figure 14*, two different peaks in water pixels can be distinguished. The far-left peak, undoubtably relates to the large body of sea water, west of the shoreline *(Figure 15).* The small peak on the right however, is arguably an indication of wet sand being incorrectly classified as water, strengthening our adjusted method. For most manually adjusted images, this turned out to be around an MNDWI pixel value of approximately -0.6.

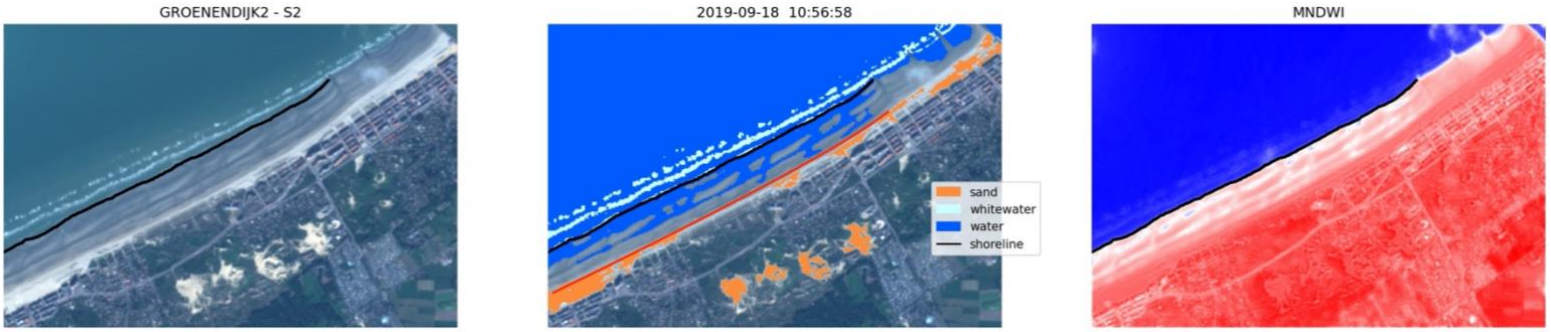

Figure 15. Accompanying image for the MNDWI histogram of Figure 9. The occurrence of wet sand at Groenendijk leads to incorrect classification of the sand/water threshold.

Secondly, the initial shoreline timeseries showed extremely large fluctuations within very short time intervals, which are highly unlikely to be correct. These various shoreline positions and their accompanying MNDWI images and pixel values were analysed. A large number of images showed a relatively wide area of white pixels in the MNDWI image, thus resulting in a wide area in which the sand-water interface can be drawn. Within this wide 'white area' the shoreline seems to be located at random by the automatic shoreline detection algorithm, possibly causing for these large and highly unlikely fluctuations in shoreline position.
To decrease these unrealistic fluctuations in the shoreline timeseries, an optimum value at the edge was chosen by hand. This value coincided with the earlier found value of ~-0.6 in the MNDWI pixel histogram. This returning value in the MNDWI histogram thus strengthens our adjusted method to manually move the land-water interface and it reduced the unrealistic fluctuations by tens of metres across all study sites.

3.3 Data Collection, Processing and Analyses

3.3.1 Collected Data Sets

Offshore wave buoy measurements provided the local water levels for the different sites, which are needed to apply a tidal correction in the last step of the CoastSat toolkit. All used data sets can be found in *Table 2*. As can be seen in the table, for three of the five locations, data from two different buoys was collected and interpolated to create local water level timeseries best suited for the study site. Table 1 gives an overview of the used buoys. The slopes required for the tidal correction, were obtained from literature and are found in Chapter 2.

For the study site of Groenendijk, no local water level data prior to 2001 were available. As stated previously the Groenendijk beach is extremely low sloping (1:100) and subject to large tidal variations, making the tidal correction highly essential for this study site. This resulted in the shoreline change analysis for Groenendijk being limited to the available water level data, thus the analysis at Groenendijk does not start until 2001.

Study site	Source	Names Buoys	Initial date available data	End date available data
Egmond aan Zee	Rijkswaterstaat (2021a)	IJgeul Stroommeetpaal	01-01-1984	31-12-2020
		Petten Zuid	01-01-1984	31-12-2020
Schiermonnikoog	Rijkswaterstaat (2021a)	Huibertgat	01-01-1984	31-12-2020
		Wierumergronden	01-01-1984	31-12-2020
Skallingen	Miljøminitriet Kystdirektoratet (2021)	Esbjerg, flyder, 6401	01-01-1998	31-12-2020
Groenendijk	Meetnet Vlaamse Banken (2021)	Nieuwpoort	01-01-2001	31-12-2020
Theddlethorpe	British Oceanographic Data Centre (BODC) (2021)	Cromer	01-01-1985	31-12-2020
		Immingham	01-01-1984	31-12-2020

Table 2. Description of water level data collected. The data is used to perform the tidal correction of the SDS shorelines in the last step of the CoastSat toolkit.

Date storms	A Duration (days)	B Maximum significant wave height (m)	C Wave direction (degrees N)	D Wave period (s)	E Wind speed (m/s)	F Wind direction (degrees N)
5 to 7 December 2013 (1)	3	7.0	240 – 360	5.0 – 13.0	8 – 26	225 – 330
21 & 22 October 2014 (2)	2	7.5	220 – 340	5.0 – 11.5	5 – 22	190 – 340
9 to 11 January 2015 (3)	3	7.0	210 – 320	4.0 – 12.0	6 – 22	190 – 300
13 & 14 January 2017 (4)	2	8.0	300 – 340	7.0 – 12.5	4 – 21	225 – 20
29 October 2017 (5)	1	7.5	280 – 360	5.5 – 12.0	7 – 26	260 – 20
3 & 4 January 2018 (6)	2	7.0	190 – 300	4.0 – 10.0	5 – 25	190 – 300
8 & 9 January 2019 (7)	2	7.0	230 – 360	4.0 – 12.0	5 – 22.5	225 – 20
9 to 12 February 2020 (8)	4	6.5	225 – 290	7.0 – 11.0	10 – 33	190 – 300

Table 3. The ten biggest storms in the North Sea during our timeseries. Given in chronological order, with the storm specific wave and wind characteristics: Colum A shows the duration of the storm in days. Colum B shows the maximum significant wave height (m); Column C shows the wave direction in degrees with respect to the North; Column D shows the wave period (s); Column E shows the wind speed (m/s); and Column F shows the wind direction in degrees with respect to the North.

To complete our shoreline analyses of long coastal stretches around the North Sea, the impact of storms on the shoreline position and morphology, must be determined. A storm response analyses based on satellite derived shorelines is entirely dependent on the frequency and availability of usable satellite images. Specifically, the time between the storm and the last pre-storm mapped shoreline as well as the first post-storm mapped shoreline is of high importance. If either of them is excessively large, no analyses of large significance can be made. The frequency of available and usable satellite images has increased hugely towards the latter stages of our timeseries, especially since the launch of Landsat 8 (2013) and Sentinel-2 (2015). Therefore, our storm response analysis was limited to these last eight years. During this time period, Rijkswaterstaat (2021b) registered eight severe storms in the North Sea. Details of the storms and their characteristics such as, significant wave height, wave direction, wave period, wind speed and wind direction (if available), can be found in *Table 3*.

As the storms used in this thesis were documented by Rijkswaterstaat (the Dutch ministry of infrastructure and water management) the storm response will be documented in relation to the Dutch coastal areas. This will show if the same storm has an impact around the entire North Sea Basin or only parts of it. It can clearly be seen in Table 2 that all storms have wind and wave directions varying between South-West to North-North-West. Eastern or north-eastern storms, which possibly have a greater impact on the shores of the United Kingdom, are not taken into account in this thesis.

It should be noted that quantifying the impact of the storm response is purely done to give an indication of the influence storms may/or may not have on the shoreline and its position. These numbers should not be seen as a value for the absolute shoreline change (erosion/accretion) per storm, as it is unknown what the actual positions of the pre- and post-storm shorelines were. This goes for all five study sites, not just Egmond aan Zee. However, knowing the number of days separating the actual pre- and post- storm shoreline positions from the ones mapped in this research, does add some perspective to the numbers. For instance, at Egmond the mapped pre-storm shoreline for storm three was mapped only two

days before the actual storm, allowing for minimal difference between the mapped and actual pre-storm shoreline.

3.3.2 Processing and Analyses

An overall mean shoreline position was calculated for each of the five study sites individually. This position was used as a reference shoreline. All shoreline positions were calculated relative to this overall mean shoreline position. Meaning: if a part of a shoreline is located landwards of the average shoreline position, this part will have a negative relative shoreline location; if a part of a shoreline is located seawards of the average shoreline location, this part will have a positive relative shoreline location.

For all five locations a linear trend and annual trends were calculated over the entire length of the timeseries, as well as a seasonal trend, which was fitted over the latter six years of all the timeseries.

4. Shoreline Change Analysis

A shoreline change analyses was done for five different study sites around the North Sea. All areas are described separately; Egmond aan Zee is discussed in Section 4.1, Schiermonnikoog in Section 4.2, Skallingen in Section 4.3, Groenendijk in Section 4.4, and Theddlethorpe in Section 4.5. The obtained results per study site have been divided into three sub-paragraphs: (1) Morphological variability; (2) Trends; (3) Storm Response.

4.1 Egmond aan Zee

4.1.1 Morphological Variability

Figure 16 shows the 2D-morphological evolution of the Egmond aan Zee shoreline from 1984 to 2020. It can be seen that the shoreline response varies hugely in the alongshore directions as well as through time. In general, the alongshore morphology can be characterized as nonuniform and does not follow a distinctive pattern.

Throughout the timescale of the analyses significant variabilities in shoreline response can be seen, both in the alongshore as cross-shore direction. The shoreline shows varying curved features, alternatingly pointed in seaward or landward direction. These various forms of horns and bays have different sizes ranging from 200 metres to 1000 meters in the alongshore direction. Two larger curves in the shoreline are visible, with the Northern curvature being the largest of the two. The distance between the two crests vary between 1.5 to 2 km. The number of minor features as well as their degrees of curvature vary through time as the beach alternates from straight to having as many as 6 adjoined minor curvatures. A straighter shoreline shape coincides with a relatively strong displacement of the shoreline position, both in on- and offshore direction.

Furthermore, at the beginning of the analyses the most Northern part is located a lot further landward than the Southern part. This dent mutates in size, varying between 500 metres and 2000 metres, as well as alongshore positions. Nevertheless, it remains present throughout the analyses and is predominantly situated in the Northern part of our study area. During the latter part of our timespan the dent moves to the South as the Northern tip advances seaward.

The Southern limit starts of as being situated further seaward than the average shoreline position. This protrusion ranges from 300 metres to 1000 metres alongshore and up to 120 metres in cross-shore, before disappearing in the latter stages of our analyses.

4.1.2 Trends

Figure 17 shows a timeseries of shoreline change at Egmond aan Zee. The mean shoreline position is seen to fluctuate around an average position, consequently there is no typical retreating or advancing trend to be distinguished. Moreover, the mean shoreline position varies over a maximum distance just shy of 100 metres throughout the entire analyses of 36 years. Short term displacements are a lot smaller and vary in size from 10 metres to 60 metres and show an increasing trend through the timeseries. Up until 2011 the displacements are only incidentally larger than 25 metres, whereas from 2015 onwards, this increases to an average displacement of around 30 metres, with a few peak displacements around 60-70 metres in the cross-shore direction.

The annual and linear trend through the entire timeseries of Egmond aan Zee can be seen in *Figure 17*. The linear trend over 37 years shows minor accretion, but shoreline change of this magnitude spread out over multiple decades is almost negligible and thus on an interdecadal scale Egmond aan Zee can be considered as a stable shoreline. The annual trend shows more fluctuations. It can be said that the shoreline goes through periods of being more landward located as well as more seaward. These more seaward or shoreward periods range between two to five years in duration and fluctuate around the linear trend. Also, the distance the annual trends deviate from the linear trend, is in the same size order for both seaward and landward excursions, but variable through time. To clarify: Shoreline excursions of a certain distance seaward of the linear trend, seem to be compensated in the next few years, with an excursion of the same magnitude in the opposite (landward) direction. *Figure 18* shows the last six years of the shoreline position timeseries for Egmond aan Zee, including the seasonal trend. In general, the shoreline is positioned further landward during autumn/winter and more seaward during spring/summer as again fluctuations dominate this trend. However, the exact duration and magnitude of these fluctuation is highly variable and do not seem to show a clear repetitive trend.

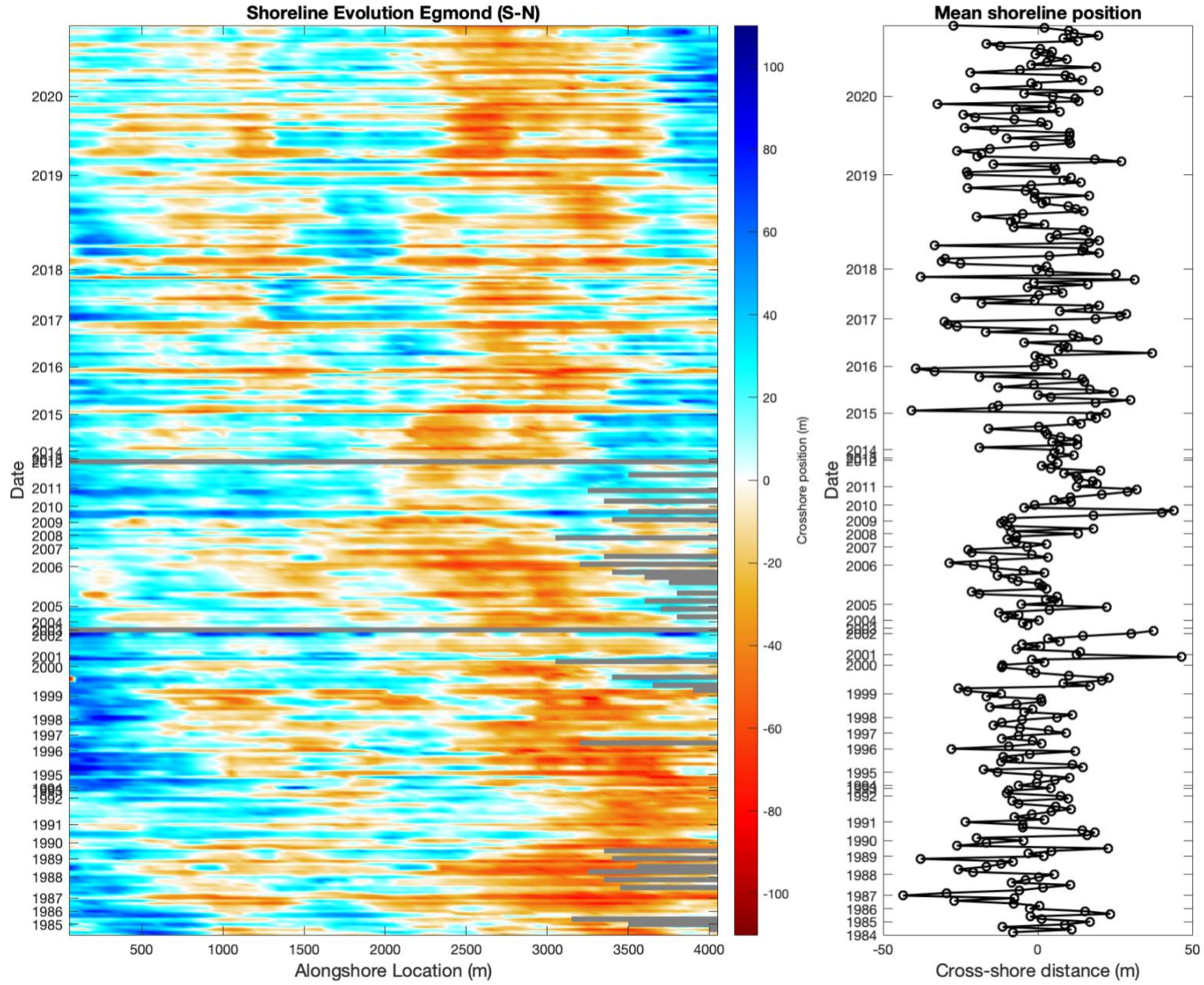

Figure 16. Shoreline evolution of Egmond aan Zee. The left-hand figure shows the shoreline position (per used satellite image) relative to the average shoreline position (x-axis), through time (y-axis). The right-hand figure shows the shoreline position, averaged in the alongshore direction (x-axis), over the same time axis (y-axis). It is important to note that the time axis is neither continuous nor linear.

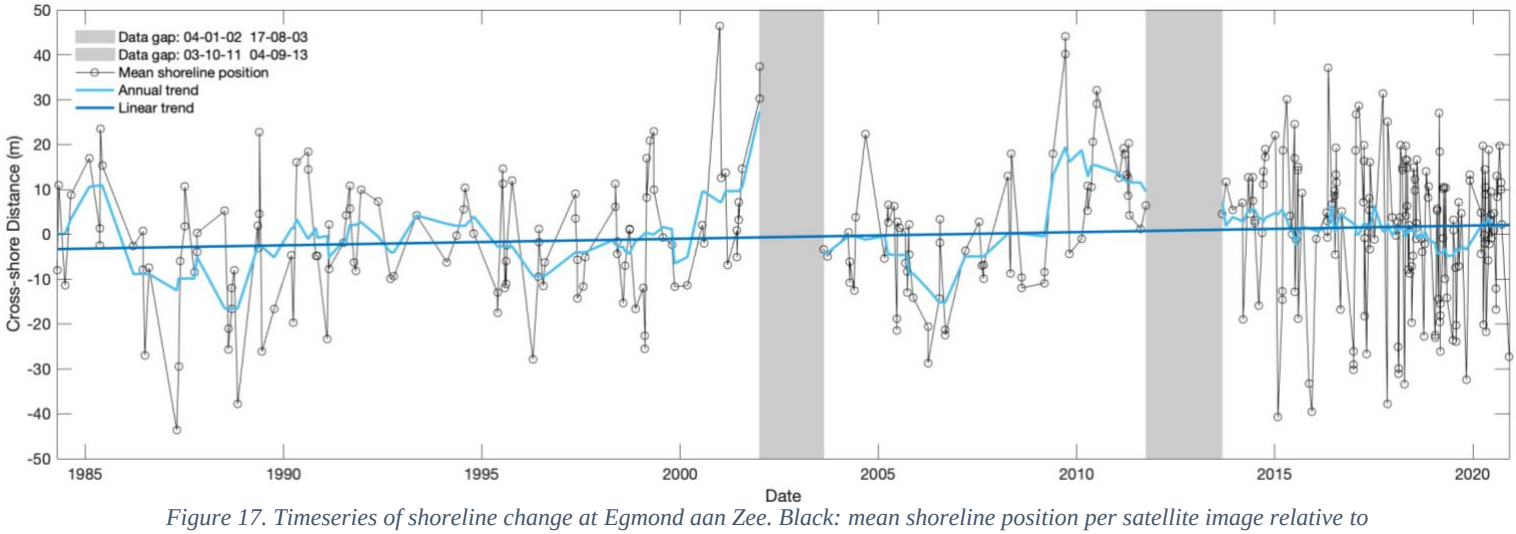

Figure 17. Timeseries of shoreline change at Egmond aan Zee. Black: mean shoreline position per satellite image relative to the total average shoreline position (zero). Red: Annual shoreline trend. Blue: linear trend through entire data set. The timeseries contains two data gaps, both comprising just over a year.

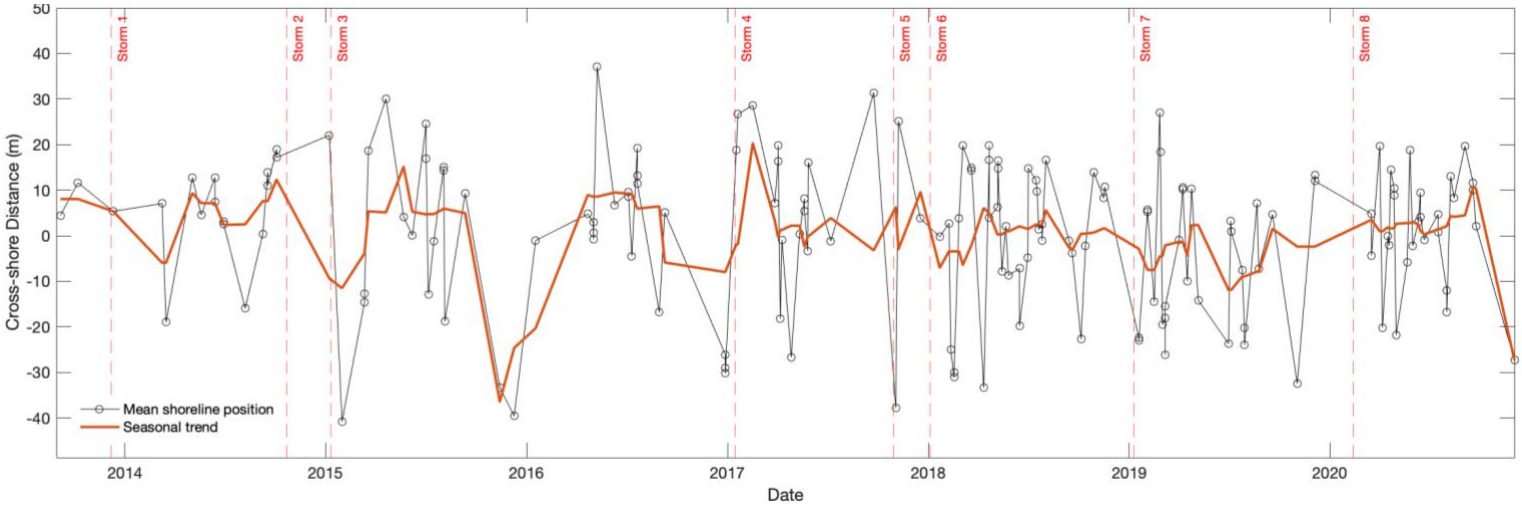

Figure 18. Timeseries of shoreline change at Egmond aan Zee. Black: mean shoreline position per satellite image relative to the total average shoreline position (zero). Orange: seasonal trend. Red: date of storm

4.1.3 Storm Response

For Egmond aan Zee, all but two (storm two and four) post-storm shorelines indicate shoreline regression (beach narrowing) after the storm, when compared to the last pre-storm shoreline. The time between the storm and the last/first pre-/post-storm mapped shoreline varies between 76 days and only 2 days, with an average of 26,4 days. *Table 4* shows the quantified difference in shoreline position based on the last/first pre-/post-storm mapped shoreline. The large amount of shoreline regression that is caused by the storms, indicates that Egmond aan Zee is susceptible to storms, specifically to storms coming from W-NW-N.

Storm	Difference between pre- and post-storm mapped shorelines (m)	Days before storm	Days after storm
5 to 7 December 2013 (1)	- 6.3	60	3
21 & 22 October 2014 (2)	+ 4.8	18	76
9 to 11 January 2015 (3)	- 62.8	2	19
13 & 14 January 2017 (4)	+ 48.7	17	2
29 October 2017 (5)	- 62.9	36	4
3 & 4 January 2018 (6)	- 4	17	7
8 & 9 January 2019 (7)	-33.1	52	9
9 to 12 February 2020 (8)	- 7.2	67	33

Table 4. Quantified difference in pre- and post-storm mapped shoreline position in meters for Egmond aan Zee, put into perspective by the number of days the shorelines are separated from the storm.

4.2 Schiermonnikoog

4.2.1 Morphological Variability

Figure 19 shows the evolution of the Schiermonnikoog shoreline from 1985 to 2020. During the timespan of our analyses the shoreline of Schiermonnikoog undergoes a few large alterations. Based on their shoreline evolution, three areas can be distinguished from one another: The North-eastern tip, the middle section and the Southwestern tip. Within these different sections there is little to no alongshore variability. It can be seen that the shoreline undergoes rotation as one tip retreats and another accretes.

Starting in the Northeast, the shoreline extends from 10500 metres up to approximately 14000 metres in 21 years (1985-2006). This is due to sand being transported onshore from a near ebb-tidal delta. This entails an enhancement of 1/3 of the length of the sandy beach. Furthermore, this north-eastern tip accretes from -575 metres to -100 metres relative to the average shoreline position during the same time span. This accretion elongates to the middle section of the study site, as this also accretes from -575 metres to -100 metres during the same time span. Meanwhile, the southwestern tip does the opposite and retreats from 450 metres to 200 metres relative to the average shoreline position. As one end retreats while the other accretes, it can be concluded the coastline of Schiermonnikoog is rotating in anticlockwise direction.
Following 2006, the north-eastern tip continuous to accrete until it reaches a maximum of 300 metres seaward of the average shoreline position in 2016, after which the area shows an alternation of accretion and regression. Relative to the average shoreline position the area is situated between -50 and 250 metres.
The middle section continuously accretes to a maximum of 100 metres seaward of the average shoreline position in 2019. However, this happens in an alternating fashion of accretion and retreat. The southwestern end of our research area shows continuous to retreat up to -50 metres, reaching this maximum/minimum in 2020.

4.2.2 Trends

Figure 20 shows a timeseries of shoreline change at Schiermonnikoog. As can be seen in the figure there are four significant data gaps at this study site. This causes difficulties when making a detailed shoreline change analysis. However, the large trend of the shoreline change is still evident. The shoreline of Schiermonnikoog shows numerous and different trends. On a year-to-year basis the shoreline fluctuated, whereas on a decadal timescale strong accretion occurs. The annual and linear trend through the entire timeseries of Schiermonnikoog can be seen in *Figure 20*. This strong accreting trend over 37 years is shown in the linear trend and compasses an average shoreline accretion of more than 200 meters. The annual fluctuations decrease is magnitude over time, indicating that most of the accretion occurred during the early stages of our analysis. From 2014 onwards the average shoreline position fluctuates between 75 metres and -50 metres, with one more landward located peak around -100 metres in March 2020. The seasonal trends (*Figure 21*) are once again of fluctuating fashion, with more seaward and shoreward periods. Nonetheless, they do not seem to be strictly linked to a season as is the case in Egmond aan Zee.

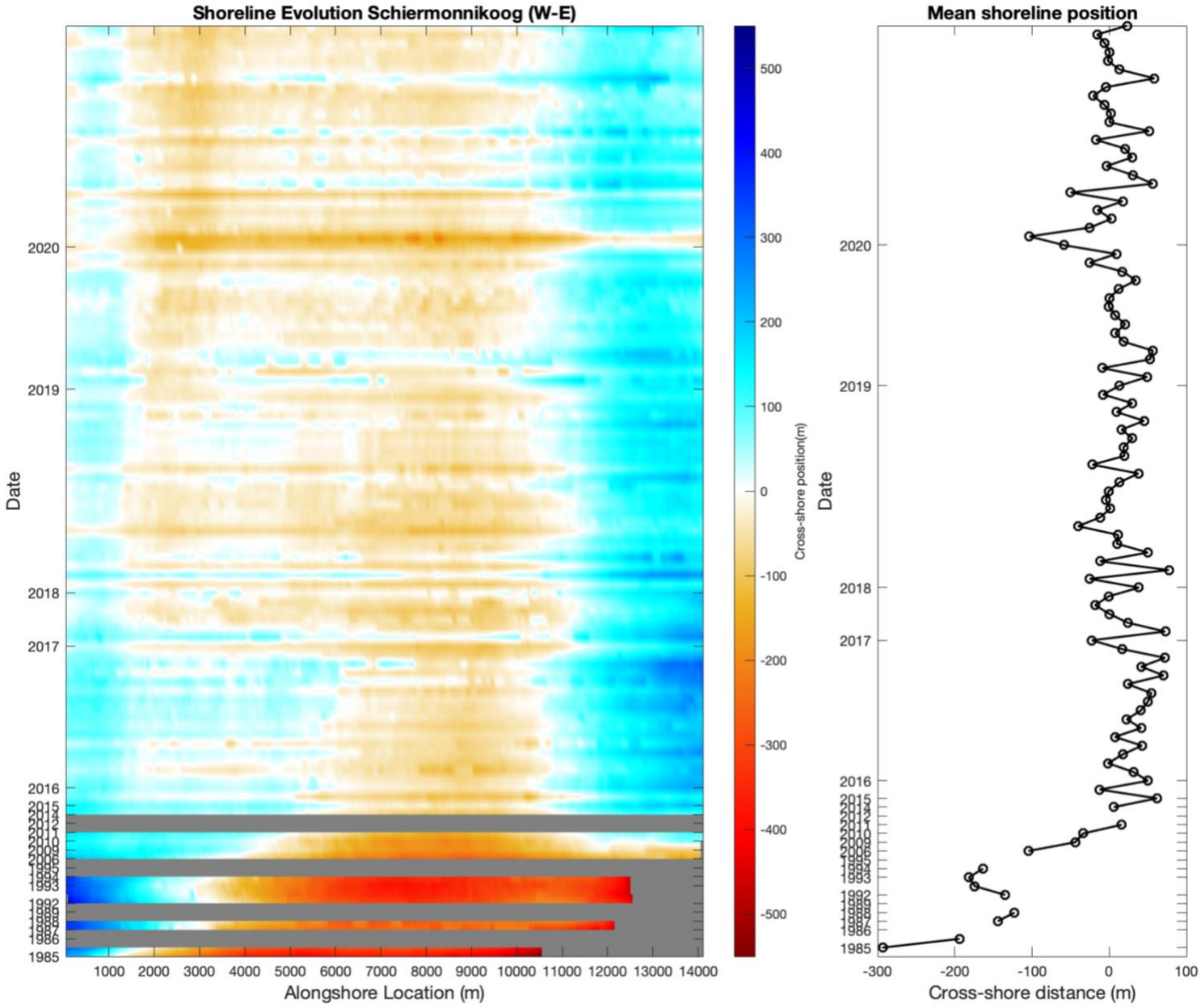

Figure 19. Shoreline evolution of Schiermonnikoog. The left-hand figure shows the shoreline position (per used satellite image) relative to the average shoreline position (x-axis), through time (y-axis). The right-hand figure shows the shoreline position, averaged in the alongshore direction (x-axis), over the same time axis (y-axis). It is important to note that the time axis is neither continuous nor linear.

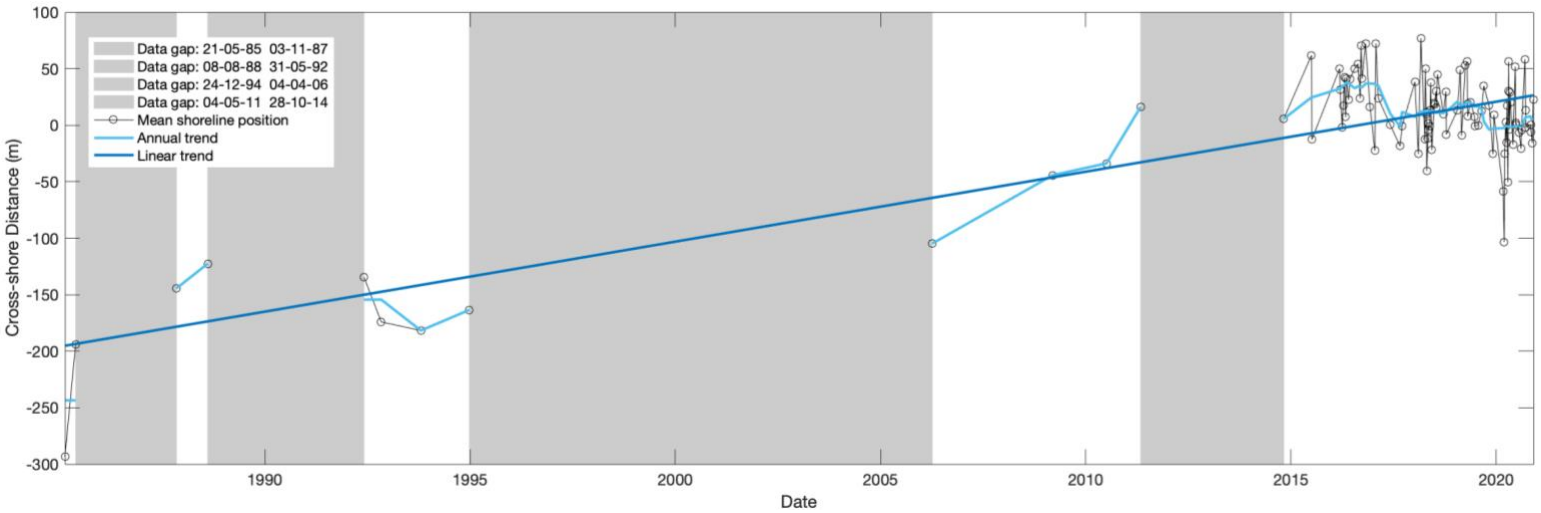

Figure 20. Timeseries of shoreline change at Schiermonnikoog. Black: mean shoreline position per satellite image relative to the total average shoreline position (zero). Red: Annual shoreline trend. Blue: linear trend through entire data set. The timeseries contains four substantial data gaps, comprising a total duration of almost twenty years.

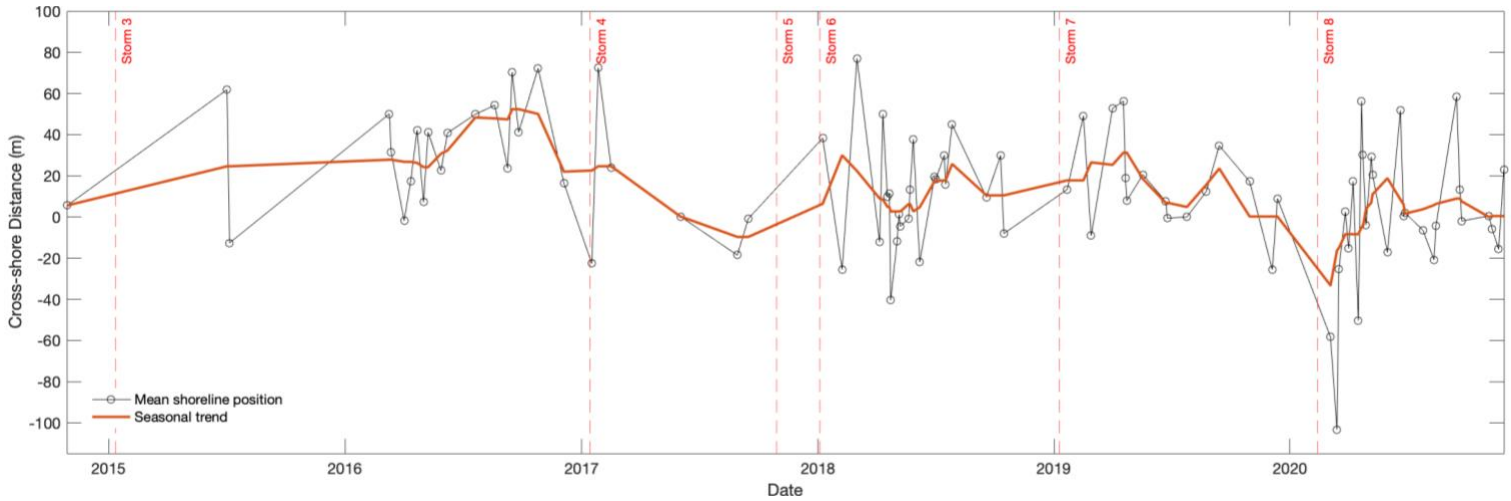

Figure 21. Timeseries of shoreline change at Schiermonnikoog. Black: mean shoreline position per satellite image relative to the total average shoreline position (zero). Orange: seasonal trend. Red: dates of storms.

4.2.3 Storm Response

The first two storms are excluded from the storm response analyses of Schiermonnikoog, as they fall within a data gap. The analysis of the barrier island is difficult to assess as the time between the storms and the pre-/post-storm mapped shorelines is substantial. The number of days between the storms and the first/last mapped shorelines, varies between 2 and 173 days, with an average of 57.6 days. Within these two months a lot of variations in shoreline position can occur, therefor the quantified difference in shoreline position from *Table 5*, are difficult to put into context. However, the two storms with the smallest time window between the mapped shorelines and the storms, storm 4 (40 days before and 2 after) and storm 8 (59 days before and 20 after), both show a negative shoreline difference indicating an eroding trend. The storms were Northwest and West orientated, respectively.

Storm	Difference between pre- and post-storm mapped shorelines (m)	Days before storm	Days after storm
5 to 7 December 2013 (1)	-	-	-
21 & 22 October 2014 (2)	-	-	-
9 to 11 January 2015 (3)	+ 56.3	73	173
13 & 14 January 2017 (4)	- 39.0	40	2
29 October 2017 (5)	+ 39.2	44	71
3 & 4 January 2018 (6)	+ 39.2	110	4
8 & 9 January 2019 (7)	+ 21.4	84	12
9 to 12 February 2020 (8)	- 67.3	59	20

Table 5. Quantified difference in pre- and post-storm mapped shoreline position in meters for Schiermonnikoog, put into perspective by the number of days the shorelines are separated from the storm.

4.3 Skallingen

4.3.1 Morphological Variability

Figure 22 shows the evolution of the Skallingen shoreline from 1984 to 2020.The shoreline adaptation is relatively uniform in the alongshore direction. Nonetheless, a clear distinction can be made between the middle section and both outer ends, based on appearance. Throughout the entire timeseries the shoreline has a curved shape, where the outer ends are positioned further seawards than the middle part. At the start of our analyses in 1984, the entire shoreline is positioned seaward of the average shoreline position. This changes to a clearly landward lying middle section and two seaward lying bulges at the ends.

Starting at the western tip, the shoreline position starts of around 250 metres seaward, compared to the average shoreline. Up to 2011 this outer end fluctuates in position between 130 metres and 250 metres relative to the average shoreline position. This is followed by a period of heavier fluctuations, where there are two brief moments where the shoreline is located landward of the average shoreline position, in 2017 and 2018. The latter part of our analyses is again characterized by fluctuations in shoreline position, which vary between 50 metres and 200 metres relative to the average shoreline position. This western tip which is characterized by this almost continuous 'positive' shoreline position, decreases in size in the alongshore direction from 2500 metres to a minimum of 500 metres towards the end of our analyses. This again, is not a steady decrease, instead it fluctuates.

The Middle section of the Skallingen shoreline is by far the largest of all three sections and is positioned just seaward at the start of our analyses. However, this changes towards a relative negative position of the shoreline, the turning point being in 2003. After this the shoreline only becomes positive on incidental occasions.

The behaviour of the eastern tip is very comparable to the western tip, but there are a few differences. Firstly, the position of the shoreline at the beginning of our analyses is further seaward, namely 300 metres seaward of the average shoreline position. During the timespan of our analyses however, the area retreats further landward than the western tip to a minimal shoreline position of -50 metres relative to the average shoreline. Lastly, the size in the alongshore direction of this 'seaward lying area' is significantly smaller, with an original size of 1000 metres to disappearing almost entirely in 2020. Having said that, the shoreline remains its curved shape throughout the entire timeseries.

4.3.2 Trends

Figure 23 shows a timeseries of shoreline change at Skallingen. Once more the shoreline position is characterized by significant fluctuations, however, a steady regressive trend is also evident. At the start of the analysis the shoreline is located around 100-150 metres seaward of the average shoreline position and shows minor fluctuations. Up until the mid-nineties, these fluctuations are relatively small and remain in the positive shoreline position region. From 1996 onwards the fluctuations become larger, and the average shoreline position attains its first negative location. Up until 2011 the average shoreline position fluctuates between 130 metres and -30 metres, with one more landward located peak around -70 metres. From 2013 onwards, the average shoreline position shows its largest variation. The shoreline positions fluctuate between 70 metres and -100 metres on average and in the latter part of the analysis, more

incidental extremes are seen. Up to 2016 the momentary displacement varies between 20 metres and 150 metres, after which there are a few very large displacements of 200 and 250 metres in 2017 and 2018. After these extreme displacements, the shoreline stabilises and the average displacement distance decreases to an average of 50 metres.

The annual timescale shows large fluctuations at the start of the timeseries, which continuously become smaller towards the end of 2020. This coincides with the overall regression slowing down. The seasonal trends are characterized by sudden, short but intense periods of a more landward positioned shoreline, alternating with longer steadier seaward positioned shorelines (*Figure 24)*. The year 2017 is a good example of this phenomena.

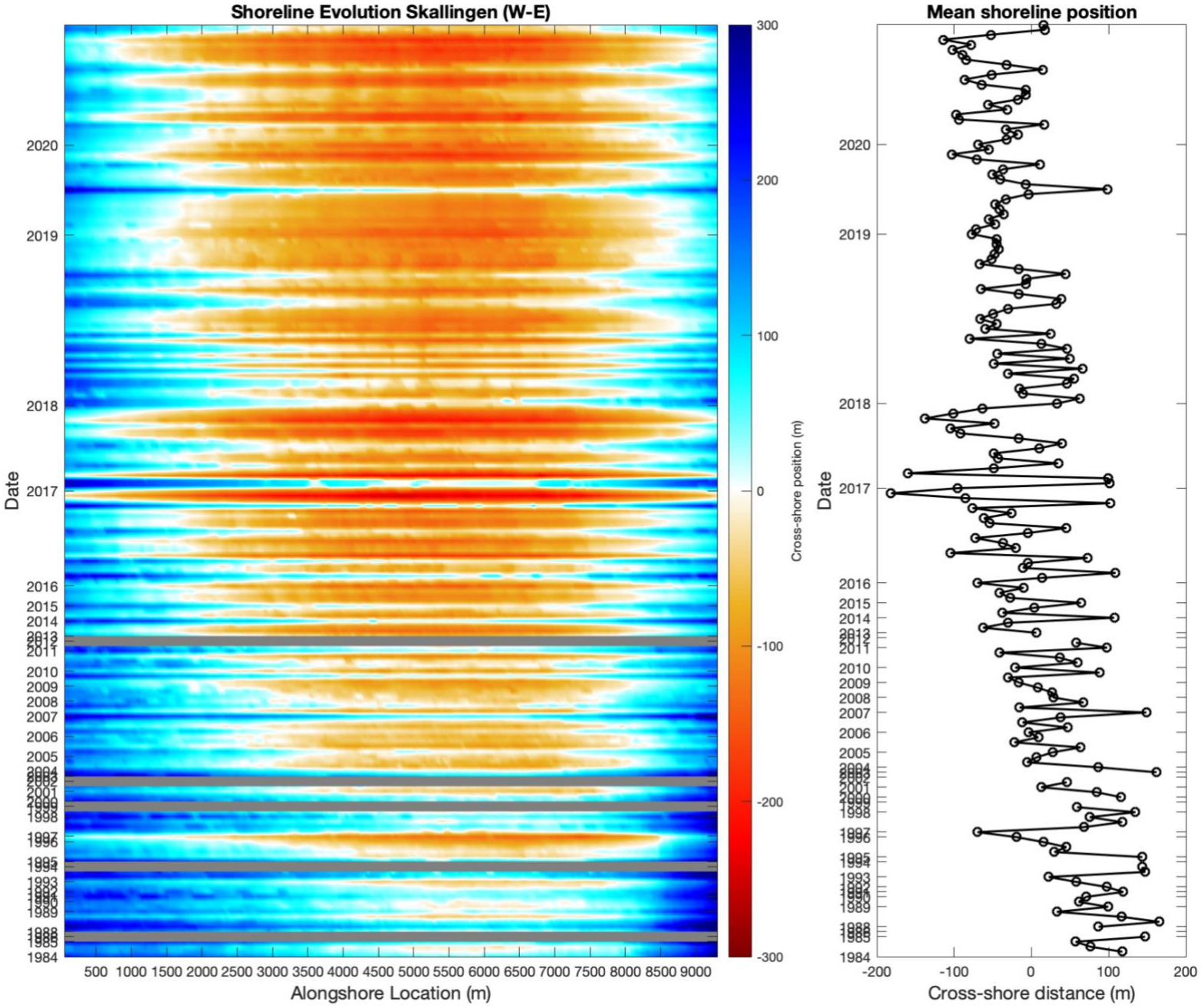

Figure 22. Shoreline evolution of Skallingen. The left-hand figure shows the shoreline position (per used satellite image relative) to the average shoreline position (x-axis), through time (y-axis). The right-hand figure shows the shoreline position, averaged in the alongshore direction (x-axis), over the same time axis (y-axis). It is important to note that the time axis is neither continuous nor linear.

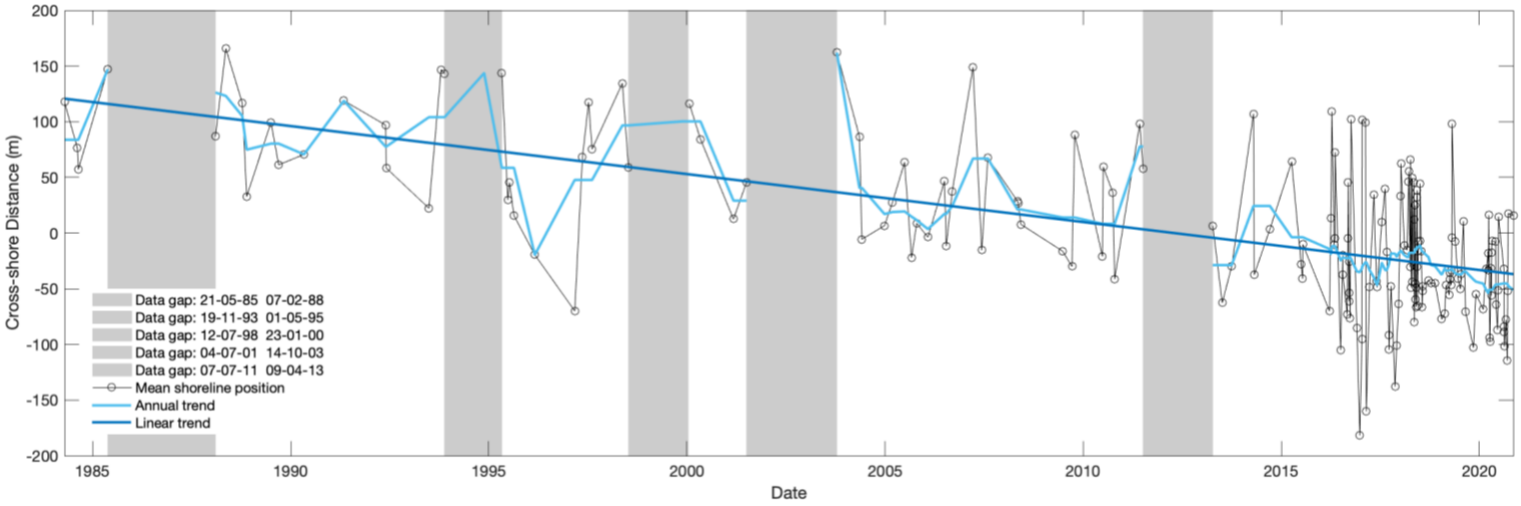

Figure 23. Timeseries of shoreline change at Skallingen. Black: mean shoreline position per satellite image relative to the total average shoreline position (zero). Red: Annual shoreline trend. Blue: linear trend through entire data set. The timeseries contains five data gaps, each comprising 1.5 to 2.5 years.

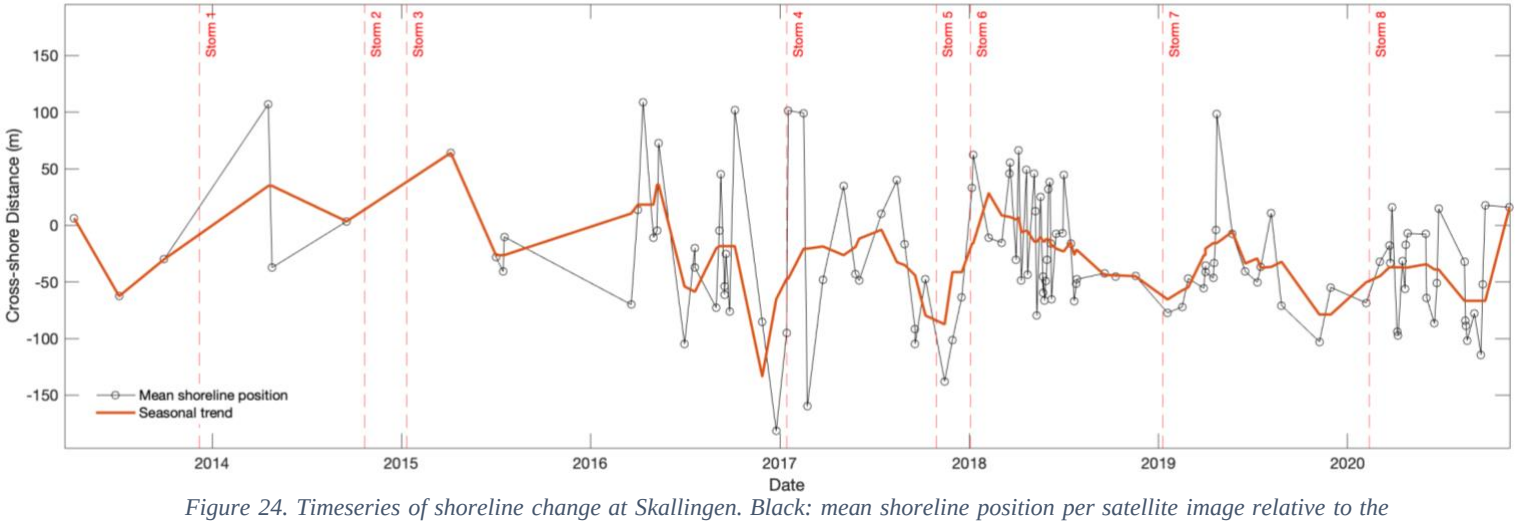

Figure 24. Timeseries of shoreline change at Skallingen. Black: mean shoreline position per satellite image relative to the total average shoreline position (zero). Orange: seasonal trend. Red: dates of storms.

4.3.3 Storm Response

The quantified difference in shoreline position at Skallingen can be found in *Table 6*. The number of days between the first/last mapped shorelines and the storms, varies between 0 and 135, with an average of 44.5. These numbers vary hugely as we have mapped shorelines from the day of the storm and two days later (storm 4), but also a time gap of more than a season before the first post-storm shorelines are mapped (storm 1 and 2). The well mapped response of the fourth storm, indicates that the Skallingen shoreline, with a NW-SE orientation, responds significantly different to the same storms than the SSW-NNO orientated shore of Egmond. The large intervals around the first three storms, speaks more of the seasonal variability, than storm response.

Storm	Difference between pre- and post-storm mapped shorelines (m)	Days before storm	Days after storm
5 to 7 December 2013 (1)	+ 137.0	67	133
21 & 22 October 2014 (2)	+ 60.5	34	135
9 to 11 January 2015 (3)	+ 60.5	114	86
13 & 14 January 2017 (4)	+ 196.7	0	2
29 October 2017 (5)	- 90.2	21	16
3 & 4 January 2018 (6)	+ 96.6	17	2
8 & 9 January 2019 (7)	- 32.6	52	9
9 to 12 February 2020 (8)	+ 36.3	4	20

Table 6. Quantified difference in pre- and post-storm mapped shoreline position in meters for Skallingen, put into perspective by the number of days the shorelines are separated from the storm.

4.4 Groenendijk

4.4.1 Morphological Variability

Figure 25 shows the evolution of the Groenendijk shoreline from 2001 to 2020. Taking a look at the shoreline evolution of Groenendijk, the area is divided into three parts: the southern, middle and northern section. Within these different sections the shoreline response is considered fairly alongshore uniform.

It is apparent that both the Southern and, to a lesser extent, Northern ends of the area show significant accretion. The middle section also shows accretion, but to lesser extent.

Starting at the Southern end, the accretion starts early in the timeseries and pushes through from 2006 onwards. The area starts of around the average shoreline position and after some retreat it begins an accreting trend, reaching its maximum seaward shoreline position of 125 metres in 2015. After having reached this maximum position, the area shows the same fluctuating trend as the entire beach shows. On average it is located seaward from the average shoreline position, with a few minor moments being further landwards than the average position. This Southern accretion reaches up to approximately 1000 metres northward.

Continuing with the middle section, it is clearly visible this area is located furthest landward, with a maximum landward position of -100 metres. Although the area does show accretion, it is never positioned very far seaward of the average shoreline position. Up until 2015 the area is stably positioned landward of the average shoreline position, after which it starts to fluctuate around the average again. These fluctuations are between -75 metres and 50 metres, relative to the average shoreline. This ‘middle landward lying area’ has an alongshore length of about 1500 metres.

Ultimately, the most Northern tip is the smallest section of all three and also shows an accreting trend. Similar to the Southern end, at the start of the timeseries the area is predominantly positioned landward of the average shoreline position, with a maximum position of -80 metres. Again, from 2015 onwards the area has accreted to an average seaward position and this is followed by fluctuations. However, these fluctuations mainly remain seaward of the average shoreline position, only reaching into the landward domain incidentally. Overall, the fluctuations during the last five years range from -40 metres to 140 metres relative to the average shoreline position.

The accretion of both tips are most likely related to the local interventions in the area. The northern tip borders a cross-shore groin, and the southern end borders an area that is frequently nourished.

4.4.2 Trends

Figure 26 shows a timeseries of shoreline change at Groenendijk. The shoreline starts of relatively steady at an average position between -40 and -60 meters between 2001 and 2004. But from 2004 onwards, the site is characterized by fluctuations and a slight accreting trend. Up until 2011 these fluctuations are minor as the shoreline position varies between -60 and 20 metres. After 2013 however, the fluctuations increase, and the average shoreline position varies between -45 metres and 60 metres. During this same period the incidental peaks in the shoreline location also increase. The short-term displacement over the entire timeseries varies between 20 metres and 110 metres and shows an increase towards the end. These short-term

displacements are large when compared to the overall shoreline accretion of only 50-75 metres. Thus indicating, Groenendijk is characterized by its heavy fluctuations. This fluctuation is most likely related to the morphology of the site, as it has a large intertidal area (>250 metres).
The sites linear accreting trend is approximately 50 meters over 20 years. As this timeseries is 'only' twenty years, which is significantly shorter than the other timeseries, there is less ground to call this a trend spanning several decades. But the speed of the accretion makes it very clear for the two decades we are analysing. The interannual trend, looks more like a multi-annual trend of varying seaward and landward positioned periods, alternating every two to four years. The seasonal trend starts off with large fluctuations, which reduce significantly in size from 2016 onwards, with the exception of one large seaward located peak in shoreline position at the end of 2018 (*Figure 27*).

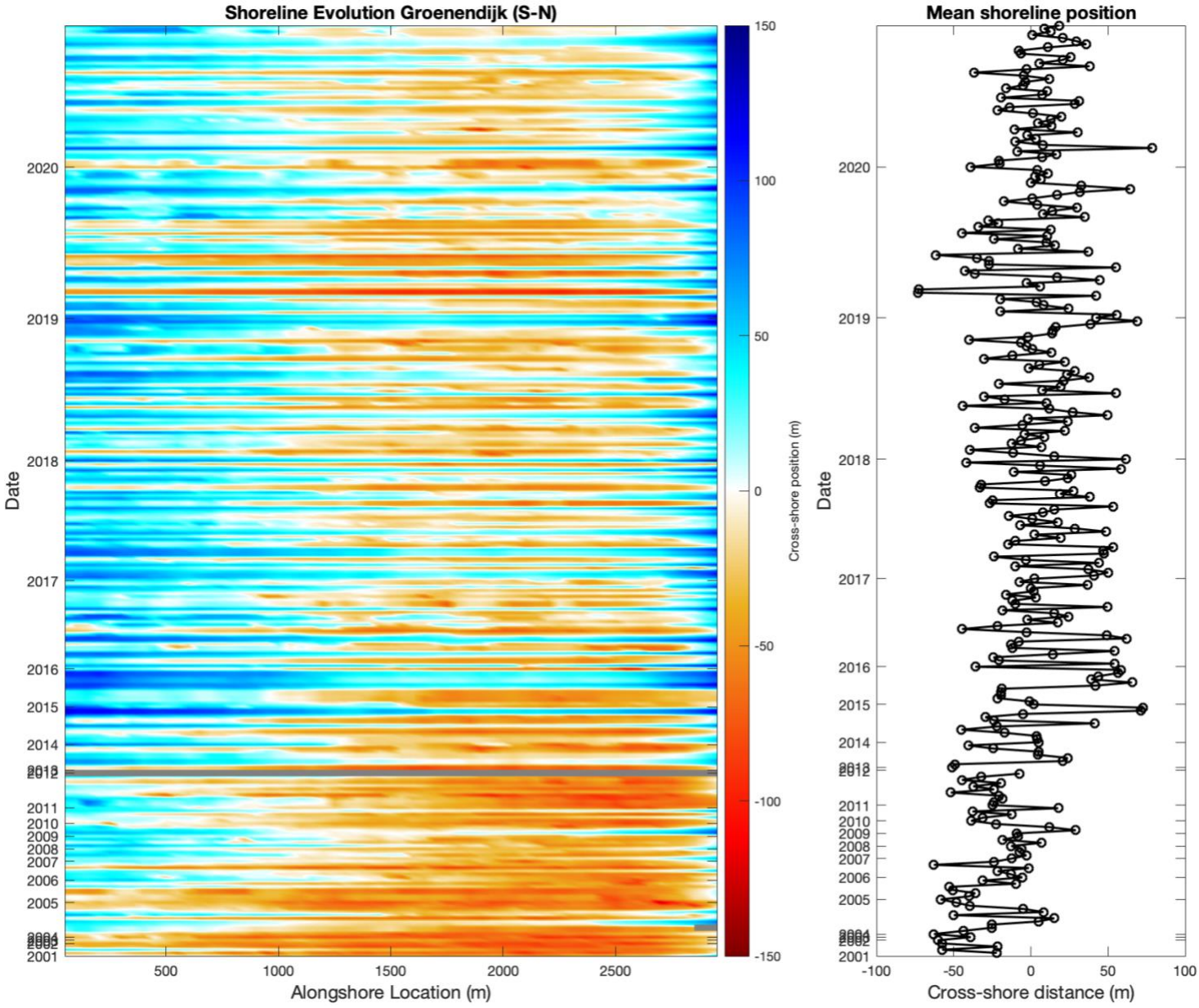

Figure 25. Shoreline evolution of Groenendijk. The left-hand figure shows the shoreline position (per used satellite image relative) to the average shoreline position (x-axis), through time (y-axis). The right-hand figure shows the shoreline position, averaged in the alongshore direction (x-axis), over the same time axis (y-axis). It is important to note that the time axis is neither continuous nor linear.

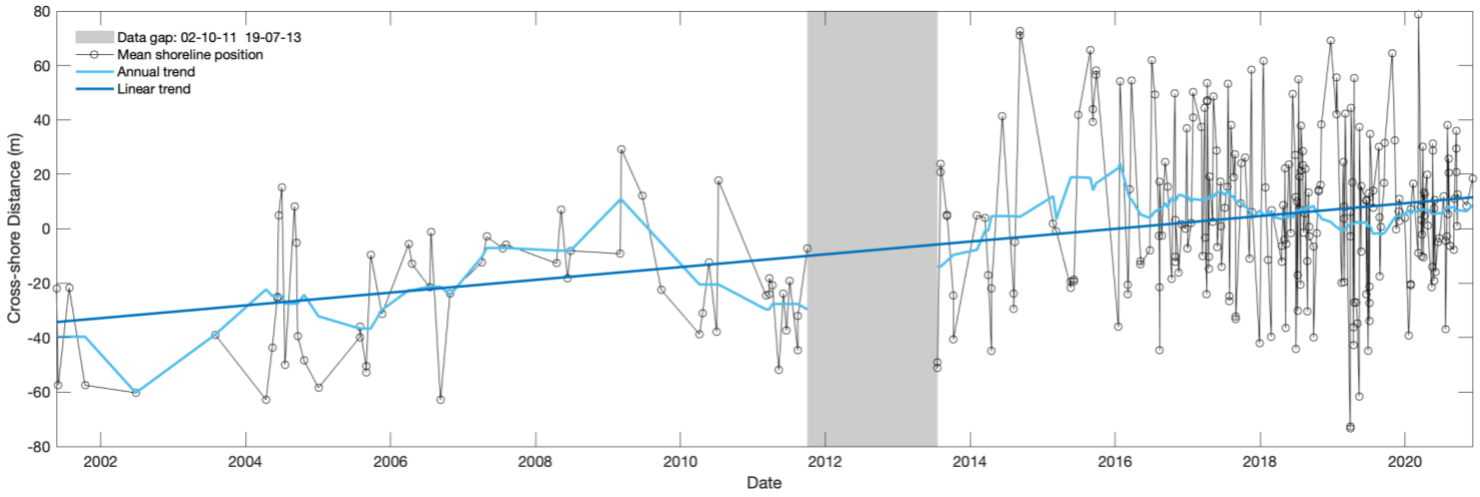

Figure 26. Timeseries of shoreline change at Groenendijk. Black: mean shoreline position per satellite image relative to the total average shoreline position (zero). Red: Annual shoreline trend. Blue: linear trend through entire data set. The timeseries contains one data gap comprising just under two years.

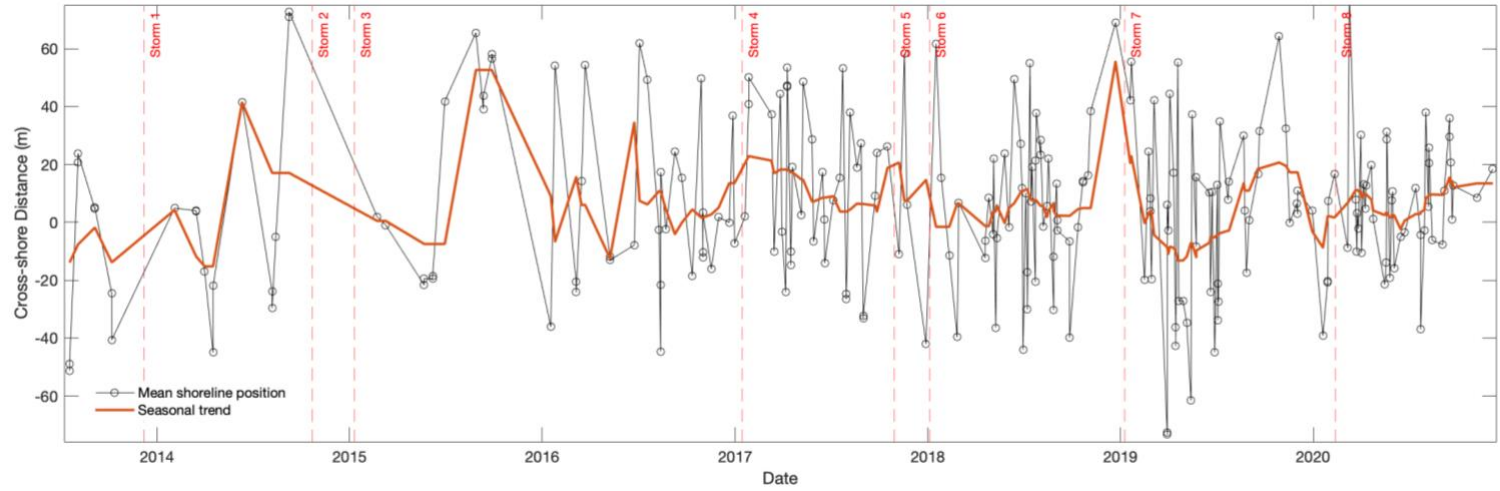

Figure 27. Timeseries of shoreline change at Groenendijk. Black: mean shoreline position per satellite image relative to the total average shoreline position (zero). Orange: seasonal trend. Red: dates of storms.

4.4.3 Storm Response

The quantified difference in shoreline position at Groenendijk can be found in *Table 7*. The number of days between the first/last mapped shorelines and the storms, varies between 0 and 123, with an average of 34.8 days. The first three storm responses are poorly mapped with long periods between the mapped shorelines and the storms. The other storms responses are better documented but show varying responses. The orientation of the Groenendijk shoreline most closely resembles the Egmond aan Zee orientation, which showed regressive trends following almost all storms. However, the storm response trend cannot directly be translated to the Groenendijk shoreline. Especially the sixth storm shows a different trend with accretion of over 100 metres.

Storm	Difference between pre- and post-storm mapped shorelines (m)	Days before storm	Days after storm
5 to 7 December 2013 (1)	+45.55	59	58
21 & 22 October 2014 (2)	- 70.8	43	123
9 to 11 January 2015 (3)	- 70.8	123	42
13 & 14 January 2017 (4)	+ 9.4	14	5
29 October 2017 (5)	- 37.3	13	9
3 & 4 January 2018 (6)	+ 103.7	6	12
8 & 9 January 2019 (7)	- 26.95	17	10
9 to 12 February 2020 (8)	-25.6	0	23

Table 7. Quantified difference in pre- and post-storm mapped shoreline position in meters for Groenendijk, put into perspective by the number of days the shorelines are separated from the storm.

4.5 Theddlethorpe

4.5.1 Morphological Variability

Figure 28 shows the evolution of the Theddlethorpe shoreline from 1984 to 2020. Taking a more detailed look at the shoreline evolution of the Theddlethorpe area, the area will be divided into two parts: the northern and southern.

Starting with the Northern half, from 1984 until 2000 the area is dominated by a slightly fluctuating, but predominantly landward positioned shoreline. These fluctuations range from -25 metres to -75 metres and are alongshore uniform. From 2001 onwards, the northern area starts to show alongshore nonuniform behaviour and can again be split in two areas. The northernmost tip shows a strong accreting trend, reaching its maximum shoreline position of 200 metres in 2010, after which it slightly retreats but still remains a positive shoreline position. The southern part of the northern half, however, remains its average landward position up until 2017. After which it starts to fluctuate around the average shoreline position, between -50 and 50 metres. The accretion in this part of the shoreline is most likely due to the evolving estuary inlet just North of our research area.

The Southern half of the Theddlethorpe area continues to fluctuate around the average shoreline position throughout the entire timeseries. However, a distinction can be made between the 1984-2000 period and 2001-2020 period. From 1984 to 2000, the southern half is mainly positioned landwards of the average shoreline position, with a few exceptions of a more seaward position. These positions vary between -70 metres and 40 metres. From 2001-2020, this switches to a predominantly seaward located shoreline, with a few landwards excursions. These excursions are very brief and as time progresses, they change from alongshore uniform to more localised and spotted areas. During this last time period the shoreline position varies between -15 metres and 130 metres relative to the average shoreline position.

4.5.2 Trends

Figure 29 shows a timeseries of shoreline change at Theddlethorpe. Again, this site shows fluctuations in the shoreline position, but to a lesser extent than the previously described beach of Groenendijk. Up until 2000 the shoreline position on average is positioned more landward and fluctuates between -75 metres and 25 metres relative to the average shoreline position. From 2000 up until 2015 the shoreline, although still fluctuating, accretes towards just seaward of the average shoreline position. From 2016 onwards the shoreline position becomes relatively stable, seaward positioned as well as less fluctuating. During this last phase of our analyses the shoreline position varies between -20 metres and 65 metres. However, our last mapped shoreline doesn’t coincide with this before mentioned steady trend and is positioned outside this range, at -46 metres. The short-term shoreline displacement of the site varies through time. From the start of our analysis up to 2016, it is relatively large at an average of 50-60 metres, with a number of occasions where it peaks beyond these distances. After 2016, the short-term displacements seldom reach beyond 40 metres.

The long-term trend of Theddlethorpe (*Figure 29*) shows accretion over a total average distance of 50 metres is 37 years. The annual trend seems to evolve during our analysis. The start of the timeseries is characterized by two-year fluctuations in shoreline position of mediocre magnitude. After the data gap these fluctuations reduce both in amplitude and duration, to almost insignificant yearly fluctuations. The seasonal trend is shown in *Figure 30* which has two mentionable landwards located peaks at the start of 2016 and the end of 2020. In between these points the trend is characterized by moderate fluctuations, slightly favouring towards more landward shoreline positions during winter and more seaward during summer.

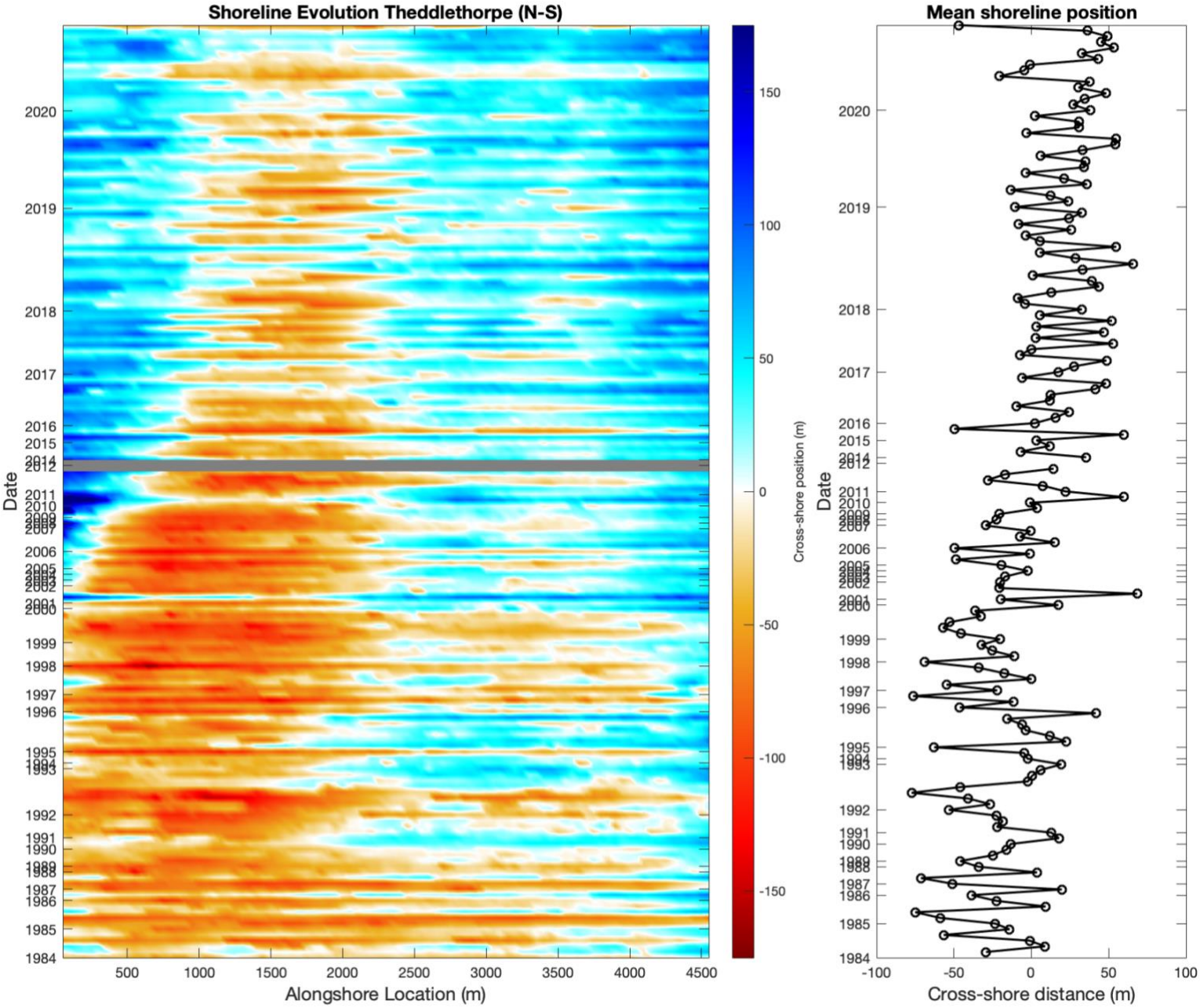

Figure 28. Shoreline evolution of Theddlethorpe. The left-hand figure shows the shoreline position (per used satellite image relative) to the average shoreline position (x-axis), through time (y-axis). The right-hand figure shows the shoreline position, averaged in the alongshore direction (x-axis), over the same time axis (y-axis). It is important to note that the time axis is neither continuous nor linear.

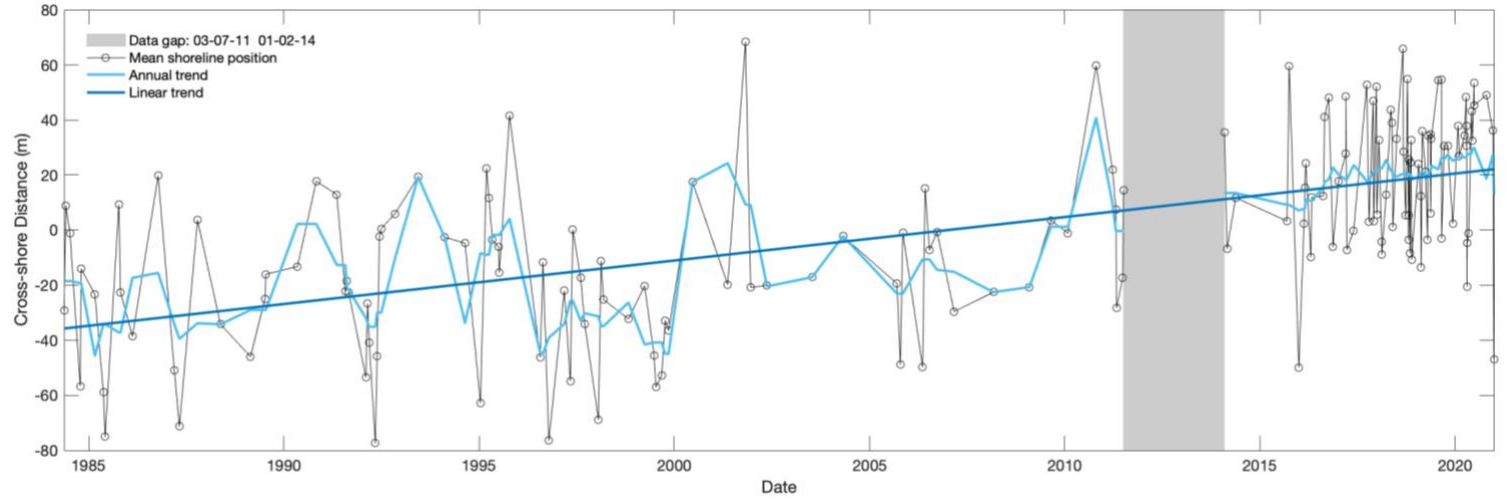

Figure 29. Timeseries of shoreline change at Theddlethorpe. Black: mean shoreline position per satellite image relative to the total average shoreline position (zero). Red: Annual shoreline trend. Blue: linear trend through entire data set. The timeseries contains one data gap comprising 2.5 years.

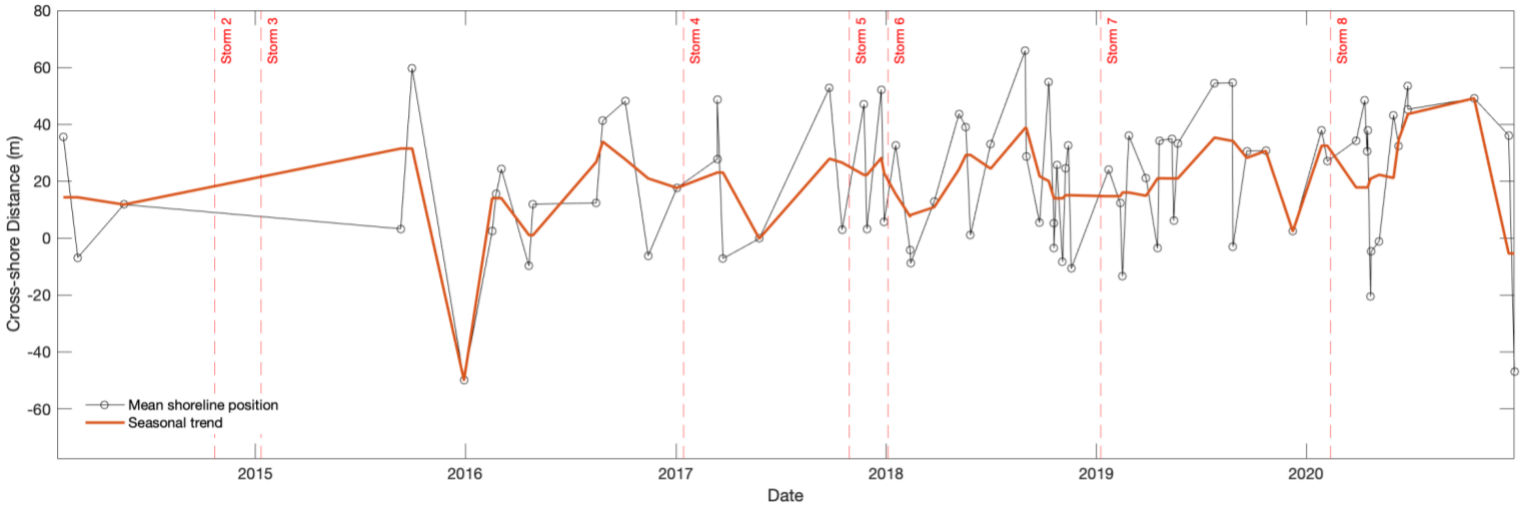

Figure 30. Timeseries of shoreline change at Theddlethorpe. Black: mean shoreline position per satellite image relative to the total average shoreline position (zero). Orange: seasonal trend. Red: dates of storms.

4.5.3 Storm Response

The quantified difference in shoreline position at Theddlethorpe can be found in *Table 8.* The number of days between the first/last mapped shorelines and the storms, varies between 3 and 322, with an average of 82.7. The first storm response cannot be documented due to data gaps, while the second and third are extremely poorly documented with more than half a year between the closest mapped shoreline and the storms. The other storms all show (slight) accreting post storm trends, a very different reaction than on the opposite side of the North Sea at Egmond aan Zee. The opposite orientation of the Theddlethorpe coast compared to Egmond aan Zee is most likely the cause for this. The storms discussed here have a common Western to Northern origin, which mainly affect the Eastern side of the North Sea Basin. Storms with a more NE-E origin will possibly have a larger effect on the Theddlethorpe shoreline. Further discussion about other storm directions can be found in Chapter 5.

Storm	Difference between pre- and post-storm mapped shorelines (m)	Days before storm	Days after storm
5 to 7 December 2013 (1)	-	-	-
21 & 22 October 2014 (2)	- 8.5	157	322
9 to 11 January 2015 (3)	- 8.5	202	242
13 & 14 January 2017 (4)	+ 10.0	9	58
29 October 2017 (5)	+ 44.0	13	25
3 & 4 January 2018 (6)	+ 27.0	6	13
8 & 9 January 2019 (7)	+ 13.3	51	13
9 to 12 February 2020 (8)	+ 7.3	3	44

Table 8. Quantified difference in pre- and post-storm mapped shoreline position in meters for Theddlethorpe, put into perspective by the number of days the shorelines are separated from the storm.

5. Discussion

Sandy coastlines are susceptible to change under the expected climate change induced developments in sea level rise, mean wave conditions and storm events. To gain further insight into the morphological response of sandy shorelines in the North Sea and the circumstances under which they occur, a shoreline behaviour analysis was done. Five study sites around the North Sea basin were analysed with the help of a new automated shoreline mapping toolkit, CoastSat. The applicability of CoastSat to the five different sites around the North Sea, was also assessed.

5.1 Applicability of CoastSat

The applicability of CoastSat is dependent on certain local circumstances and factors. The first factor is the local tidal range, which influences the correctness of the mapped shorelines. In areas where the water level shows little to no tidal variations, the shorelines produced by CoastSat do not need to be corrected or adjusted for varying water levels. This relation increases in areas with a steep slope (i.e. small intertidal area), where varying water levels, if at all present, will not cause for large shoreline displacements. These specific characteristics make up the ideal study site for the use of CoastSat.
If we compare this to the opposite circumstances (i.e. meso or macro-tidal low sloping beach with a large intertidal area) the use of CoastSat becomes increasingly complicated. Areas with a large tidal range, undergo significant water level variations, affecting the instantaneous position of the shoreline: high water results in a further landwards located shoreline and low water moves the shoreline seaward). Satellite images are taken at various moments throughout the tidal cycle, meaning the mapped shorelines are subject to these altering positions and need proper adjustment. Quantifying these tidal corrections, subjects the mapped shorelines to errors as external data is required to perform the corrections, such as local water level and beach slope.

Furthermore, local morphology also influences CoastSat's ability to determine the exact shoreline position. As explained previously (Chapter 3) the position of certain shorelines had to be adjusted manually, as the automated shoreline detection algorithm mistook the transition from wet to dry sand as the sand/water interface. Low sloping beaches with a large intertidal area are significantly more susceptible to these implications than steeper beaches as the water simply reaches a lot less further up the beach. This also regards the wave runup, which can vary per location and is also subject to variations induced by the local wave climate. A recent study by Castelle et al. (2021) showed that including wave runup is crucial in improving the estimation of the shoreline position. Including set-up only caused minor improvement, which was surprising as it is extremely unlikely that most satellite images were taken at the time of maximum runup. The paper states that wet sand is most likely the main source for these errors, which coincides with our preliminary findings of CoastSat's applicability (Chapter 3).

A combination of both the tidal range and local morphology which hampers the automated shoreline detection is the occurrence of large intertidal sandbars, as is the case at Groenendijk, Egmond aan Zee and Theddlethorpe. A lower water level can lead to a fluctuating shoreline

position as the water positions itself in between the near shore sandbars. This oscillating line however is not true to the real shoreline, meaning these shorelines also must be manually adjusted.

A last factor concerning the applicability of CoastSat is the number of suitable satellite images available per location. Schiermonnikoog has numerous large data gaps comprising more than half (twenty years) of the timeseries, significantly affecting the amount to which the shoreline change can be analysed. However, this implication is more related to satellite coverage and local weather conditions than the functioning of the CoastSat toolkit.

5.2 Shoreline analyses

All study sites show large short-term fluctuations in shoreline position, varying between 10-60 meters, with a few extremes exceeding 100 meters. The short-term fluctuations are also found in previous studies concerning satellite derived shorelines (Castelle et al., 2021; Luijendijk et al., 2018). However, the magnitude is usually more around 20 – 40 metres. Especially a portion of the fluctuations found in this research is questionable (~ 200 metres within 10 days at Skallingen). As mentioned previously, not including the wave runup can be a significant source of error as well as the incorrect classification of wet sand as water. These are plausible explanations of these large variations. Another explanation for this large fluctuation is the large dependency on external data sets for tidal correction, leaving the satellite derived shorelines susceptible to errors even after the correction was applied. Local water levels of the closest available buoys were used, nonetheless these are not always in the nearby area. The average distance from the used buoys to the study site is 15 kilometres.

Furthermore, the long-term average shoreline positions and the filtering of the time-series are significantly dependent on the interval between two usable satellite images and mapped shorelines. Therefor determining rates of shoreline change becomes difficult for the shorter trends on the temporal scale, whereas towards the longer end of the temporal scale trends are easier to quantify. The detection of storm response is highly dependent on the satellite coverage and is almost impossible if this is low. Therefore, the shoreline change values noted in *Tables 4-8* are put into perspective in *Figure 31* and *Figure 32.*

The Figures display the average difference between pre- and post-storm mapped shorelines (y-axis) over the average number of days between a storm and the first/last mapped pre-/post-storm shoreline (x-axis), including the standard deviations. As can be seen the figures contain a lot of scatter and no clear trend can be seen in either of the figures. Also, the standard deviations are rather large meaning the data is prone to a large window of error.

Therefor it can be said that the impact of a single storm can be spotted, but the frequency of the satellite images available for our research areas is not sufficient to quantify and determine the exact shoreline storm response. However, the influence of storms to the overall trend can still be determined. This topic will be explained in more detail in Section 5.3.

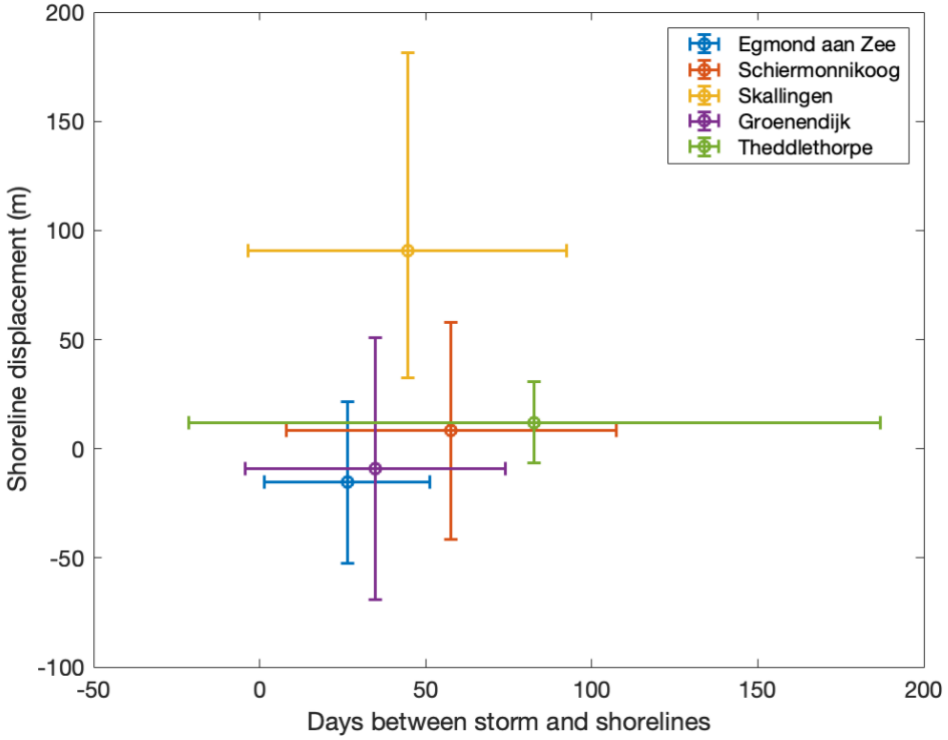

Figure 31. Statistical storm coverage analyses per research area. The average difference between pre- and post-storm mapped shorelines (y-axis) over the average number of days between a storm and the first/last mapped pre-/post-storm shoreline (x-axis). The standard deviations are included as error bars in the figures.

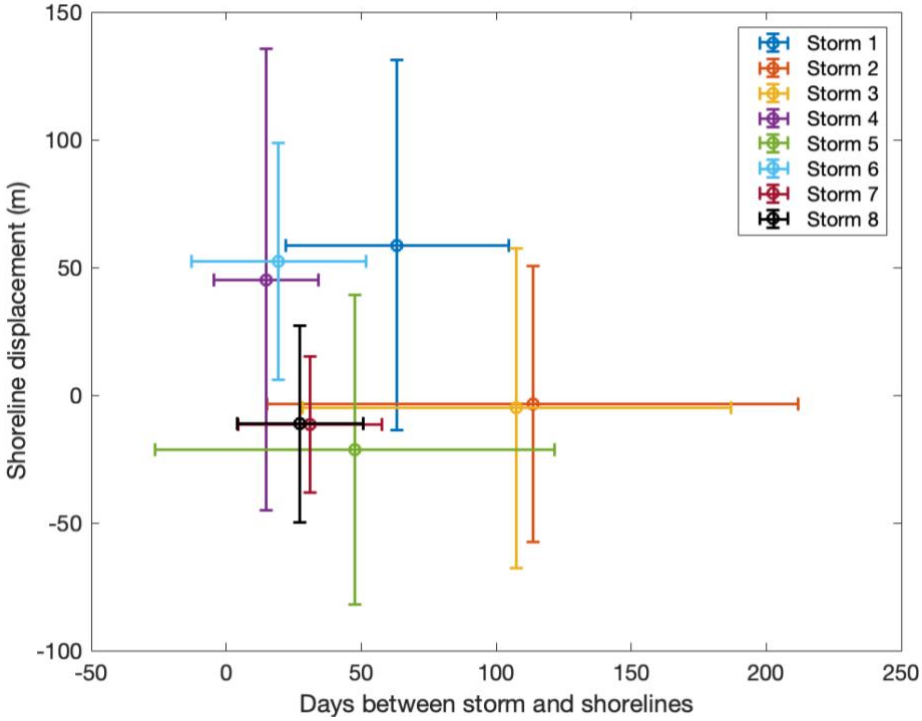

Figure 32. Statistical storm coverage analyses per storm. The average difference between pre- and post-storm mapped shorelines (y-axis) over the average number of days between a storm and the first/last mapped pre-/post-storm shoreline (x-axis). The standard deviations are included as error bars in the figures.

5.3 Coastal change around the North Sea

All five study sites are located within the same North Sea basin and are, in large amounts, subject to the same weather circumstances. Despite this, all study sites show large variations in shoreline behaviour. All five locations exhibit long-term trends in shoreline position and morphological change.

The position of the shoreline of Egmond aan Zee remains stable when considering the long-term trend, nonetheless it fluctuates on a seasonal and annual basis. This fluctuation is most likely linked to the finding that exposed sandy beaches are dominated by seasonal variability in cross-shore sediment processes (Masselink et al., 2016; Scott et al., 2016) This explanation of seasonal variability can also be applied to Schiermonnikoog, Groenendijk and Theddlethorpe as they are all unsheltered shorelines.

This site also shows alongshore variability, in the form of two main curvatures in the shoreline, with a spacing between the two megacusps varying between 1000 to 2000 metres. Peuziat (2017) found a similar spacing between the horns of the crescentic outer bars at Egmond aan Zee. This implies that the shoreline of Egmond aan Zee is coupled to the local bar system, causing alongshore variability of the shoreline. As locating the position and shape of the nearshore bar morphology was not a part of this thesis, we cannot determine if the coupling is in- or out-of-phase, based on the knowledge gained here. Previously presented work by António (2017) has found the coupling at Egmond aan Zee to be predominantly in phase. These megacusps seem to flatten with heavy shoreline changes and following numerous of our researched storms. Nearshore bar morphology at Egmond is known to show cyclic behaviour and is also influenced by high wave events (i.e. storms) (Ruessink et al., 2009).

Schiermonnikoog shows an accreting and anti-clockwise rotating trend. The accreting trend was previously suggested and shown by Prakken (1989) and Stive (2002) up to the change of the century, whereas this research shows that the accreting trend continues throughout the first twenty years of the 21st century and possible longer. The reason for this accretion is most likely the attachment of sandy shoals from the ebb-tidal delta (*Figure 33*). The attachment of an ebb-tidal delta on this Eastern end of Schiermonnikoog is a typical characteristic for such tidal inlets. The distortion and movement of the shoal(s), as well as it's bent-shaped attachment, resembles the morphological activity of the shoal attachment onto Langeoog from the Accumer ebb-tidal delta (*Figure 3*). Here the shoals are also seen to bend around the island head. Although exact migrations speeds for the sandy shoals attaching Schiermonnikoog are not known, the images of *Figure 33* suggest that these shoals show the same slowing migration trend closer to the shore as the shoals of the Accumer Ee ebb-tidal delta.

Skallingen is the only shoreline which shows significant retreat. The size of the retreat indicates the cause being sediment related. This is supported by numerous literature studies (Aagaard et al., *2004b*; Christiansen et al., 2004). The effect storms have on the shoreline are dependent on the local morphology. The Skallingen shoreline seems to broaden during the storms analysed in this thesis (*Table 6*), instead of leading to erosion. Christiansen et al. (2004) found that during storm surges, the nearshore sandbars migrate in onshore direction up to 20-30 metres per event,

causing short term shoreline progradation. This onshore bar migration simultaneous leads to a significant steepening of the shoreface, which on its own leads to a weaker shoreface, as the waves break further shoreward, resulting in shoreline erosion. This alternating trend of accretion and erosion described by Christiansen et al. (2004), is also observed in the results presented in Section 5.3. However, the shoreline has an overall strong transgressive trend due to substantial sediment losses to longshore transport, towards the southeast, into the nearby estuaries and due to the lack of sediment gain from the northwest due to the existing groyne field trapping the sediment further up alongshore. Groynes are most likely also the reason for the curved shape of the shoreline. Both ends of our research area are bordered by a cross-shore positioned groyne (*Figure 9*), trapping sediment, or sheltering the area from longshore transport. Further away from these groynes the shoreline becomes more exposed to the longshore currents causing erosion.

The Groenendijk shoreline is characterized by large seasonal fluctuations and a small accreting trend. Although the research area itself, has not been subject to nourishments, the beaches just south of Groenendijk have been regularly nourished (Pranzini & Williams, 2013). Alongshore

Figure 33. Satellite images showing the migration and attachment of sandy shoals to the north-eastern head of Schiermonnikoog from 1985 to 2020 (Google Earth Engine, 2021).

sand distribution from these nourishments by the Lee and Feeder effect is most likely the cause of this accretion. The Northern tip of the Groenendijk shoreline also borders a cross-shore groyne causing for a disruption of the local sediment transport. The shoreline bordering the groyne is thus located further seaward, as the groyne functions as a small sediment trap.

The Theddlethorpe area is characterized by fluctuating shoreline positions as well as a slight accretion. Van Houwelingen et al. (2006), state that this part of the North Lincolnshire coast is characterised by seasonality in the wind and wave climate, leading to seasonal and annual fluctuations of the shoreline position. The more seaward position of the norhern end is most likely linked to the nearshore morphology as the slope decreases towards the North (Van Houwelingen et al., 2006). This low gradient causes the wave height to be significantly smaller towards the North of our study area, resulting in less wave breaking and a more shoreward position of the shoreline. This northward decreasing slope causes the area to the south of this 'shelf' to be more susceptible to shoreline erosion, indeed resulting in a more landward directed shoreline (*Figure 28*).

Furthermore, the impact of single storm events is visible at certain study areas, but they do not lead to system change and do not seem to dominate the long-term trends of the shoreline position. They merely cause minor fluctuations on a short-term scale. This can be said because all sites show steady annual and seasonal trends throughout the entire timeseries, without major incidental interruptions (other than data gaps). At Skallingen storm surges do seem to affect the near-shore bar morphology, causing short-term shoreline fluctuations, although this still doesn't change the long-term erosive trend of the site. Thus, it can be said that adaptation of the shoreline seems strongly dependant on local factors (described for each site above), such as morphology, orientation, local wave climate and coastal management strategies, rather than storm events. However, the shoreline change in this thesis is primarily focused on the 2D position of the shoreline. Sediment volumes (whether subaerial or subaqueous) and their change are not considered here. This means that dune erosion or erosion of the nearshore sandbars, cannot be determined with the use of CoastSat.

5.4 Recommendations

In this thesis the focus was put primarily on gaining insight in shoreline change around the North Sea and not on improving a shoreline detection algorithm. To improve the accuracy of the shoreline detection algorithm a few alterations can be made, which are: including the wave runup; including a sandbank detection algorithm, which eliminates the oscillation in the shoreline due to the nearshore banks; retraining the supervised classification to local areas including large areas of wet sand; adding other sources for satellite images, and thus increasing the frequency of available images.
Furthermore, the storms considered in this research are mainly focused and selected on the impact the storms had on the Dutch Coastal areas, and thus only include storms from southwestern to northern origin. For a completer analysis, storms from all origins should be considered as they will most likely show other relations at the non-Dutch sites.

6. Conclusion

This MSc thesis aimed at improving understanding of shoreline behaviour at various spatial and temporal scales at contrasting sites around the North Sea, while also testing the applicability of CoastSat to these various sites around the North Sea. This was done with the help of an open-source software toolkit, CoastSat, which semi-automatically maps shorelines from 1984 to the present. We analysed five sandy beaches around the North Sea with varying tidal ranges orientations and wave exposure.

We found that all locations exhibit long-term trends in shoreline position and morphological change. These trends show large variations between the different sites and are characterized by local factors such as morphology, orientation, local wave climate and coastal management strategies. Summing up we see: (1) a steady cross-shore shoreline position at Egmond aan Zee; (2) rotation in the anti-clockwise direction combined with accretion of more than 200 meters at Schiermonnikoog; (3) Strong shoreline erosion of more than 150 meters at Skallingen; (4) Accretion of 25 meters at Groenendijk; and (5) shoreline accretion of 60 meters at Theddlethorpe. Alongshore variations in the shoreline are caused by specific local circumstances and are thus site specific. The impact of single storm events is visible, but they do not lead to system change and do not dominate the long-term trend as they merely cause minor fluctuations on a short-term scale. Furthermore, the applicability of CoastSat varies around the North Sea. This variance is mainly dependent on the beach slope, tidal regime, local morphology, and satellite image availability.

The time scale of the shoreline change allowed for determining detailed long-term shoreline change around different areas along the North Sea. Site specific findings as well as general trends concerning the entire basin were presented. Mapping accurate and quantifiable storm responses was not possible due to the low frequency of satellite images. Including a database with a higher frequency of satellite images in future work will help to determine storm response accurately.

References

Aagaard, T. (1988). Rhythmic beach and nearshore topography: Examples from Denmark. *Geografisk Tidsskrift-Danish Journal of Geography*, *88*(1), 55-60.

Aagaard, T. (2002). Modulation of surf zone processes on a barred beach due to changing water levels; Skallingen, Denmark. *Journal of Coastal Research*, 25-38.

Aagaard, T., Davidson-Arnott, R., Greenwood, B., & Nielsen, J. (2004a). Sediment supply from shoreface to dunes: linking sediment transport measurements and long-term morphological evolution. *Geomorphology*, *60*(1-2), 205-224.

Aagaard, T., Kroon, A., Andersen, S., Sørensen, R. M., Quartel, S., & Vinther, N. (2005). Intertidal beach change during storm conditions; Egmond, The Netherlands. *Marine geology*, *218*(1-4), 65-80.

Aagaard, T., Nielsen, J., Jensen, S. G., & Friderichsen, J. (2004b). Longshore sediment transport and coastal erosion at Skallingen, Denmark. *Geografisk Tidsskrift-Danish Journal of Geography*, *104*(1), 5-14.

Anthony, E. J. (2013). Storms, shoreface morphodynamics, sand supply, and the accretion and erosion of coastal dune barriers in the southern North Sea. *Geomorphology*, *199*, 8-21.

António, S.D. (2017). Shoreline and sandbar coupling on a natural and nourished beach. *MSc Thesis.*

ArcGIS (2021). Retrieved on 19-04-2021. Retrieved from: https://pro.arcgis.com/en/pro-app/latest/tool-reference/data-management/generate-transects-along-lines.htm

Arens, S. M. (1994). Aeolian processes in the Dutch foredunes, PhD Dissertation, University of Amsterdam, 31-37.

Bakker, J. P., Veeneklaas, R. M., Jansen, A., & Samwel, A. (2005). Een nieuw groen strand op Schiermonnikoog. *De Levende Natuur*, *106*(4), 151-155.

Boak, E. H., & Turner, I. L. (2005). Shoreline definition and detection: a review. *Journal of coastal research*, *21*(4 (214)), 688-703.

BODC (2021). Retrieved on 18-01-2021. Retrieved from: https://www.bodc.ac.uk/data/hosted_data_systems/sea_level/uk_tide_gauge_network/processed/

Brand, E., Montreuil, A. L., Houthuys, R., & Chen, M. (2020). Relating Hydrodynamic Forcing and Topographic Response for Tide-Dominated Sandy Beaches. *Journal of Marine Science and Engineering*, *8*(3), 151.

Castelle, B., Bonneton, P., Dupuis, H., & Sénéchal, N. (2007). Double bar beach dynamics on the high-energy meso-macrotidal French Aquitanian Coast: a review. *Marine geology*, *245*(1-4), 141-159.

Castelle, B., Guillot, B., Marieu, V., Chaumillon, E., Hanquiez, V., Bujan, S., & Poppeschi, C. (2018). Spatial and temporal patterns of shoreline change of a 280-km high-energy disrupted sandy coast from 1950 to 2014: SW France. *Estuarine, Coastal and Shelf Science*, *200*, 212-223.

Castelle, B., Marieu, V., Bujan, S., Splinter, K. D., Robinet, A., Sénéchal, N., & Ferreira, S. (2015). Impact of the winter 2013–2014 series of severe Western Europe storms on a double-barred sandy coast: Beach and dune erosion and megacusp embayments. *Geomorphology*, *238*, 135-148.

Castelle, B., Masselink, G., Scott, T., Stokes, C., Konstantinou, A., Marieu, V., & Bujan, S. (2021). Satellite-derived shoreline detection at a high-energy meso-macrotidal beach. *Geomorphology*, *383*, 107707.

Castelle, B., Ruessink, B. G., Bonneton, P., Marieu, V., Bruneau, N., & Price, T. D. (2010). Coupling mechanisms in double sandbar systems. Part 1: Patterns and physical explanation. *Earth Surface Processes and Landforms*, *35*(4), 476-486.

Chander, G., Markham, B. L., & Helder, D. L. (2009). Summary of current radiometric calibration coefficients for Landsat MSS, TM, ETM+, and EO-1 ALI sensors. *Remote sensing of environment*, *113*(5), 893-903.

Christiansen, C., Aagaard, T., Bartholdy, J., Christiansen, M., Nielsen, J., Nielsen, N., ... & Vinther, N. (2004). Total sediment budget of a transgressive barrier-spit, Skallingen, SW Denmark: A review. *Geografisk Tidsskrift-Danish Journal of Geography*, *104*(1), 107-126.

Davidson, M. A., Splinter, K. D., & Turner, I. L. (2013). A simple equilibrium model for predicting shoreline change. *Coastal Engineering*, *73*, 191-202.

De Moor, G., Ozer, A. and Heyese, I., 2010. Belgium. In *Encyclopedia of the World's Coastal Landforms.* Springer Science, Dordrecht, 669–671.

De Schipper, M. A. (2014). Alongshore variability of nourished and natural beaches.

De Schipper, M. A., de Vries, S., Ruessink, G., de Zeeuw, R. C., Rutten, J., van Gelder-Maas, C., & Stive, M. J. (2016). Initial spreading of a mega feeder nourishment: Observations of the Sand Engine pilot project. *Coastal Engineering*, *111*, 23-38.

De Vriend, H. J., van Koningsveld, M., Aarninkhof, S. G., de Vries, M. B., & Baptist, M. J. (2015). Sustainable hydraulic engineering through building with nature. *Journal of Hydro-environment research*, *9*(2), 159-171.

De Winter, R. C., Gongriep, F., & Ruessink, B. G. (2015). Observations and modeling of alongshore variability in dune erosion at Egmond aan Zee, the Netherlands. *Coastal Engineering*, *99*, 167-175.

Del Río, L., Gracia, F. J., & Benavente, J. (2013). Shoreline change patterns in sandy coasts. A case study in SW Spain. *Geomorphology*, *196*, 252-266.

Deronde, B., Houthuys, R., Debruyn, W., Fransaer, D., Lancker, V. V., & Henriet, J. P. (2006). Use of airborne hyperspectral data and laserscan data to study beach morphodynamics along the Belgian coast. *Journal of Coastal Research*, *22*(5 (225)), 1108-1117.

Ducrotoy, J. P., Elliott, M., & de Jonge, V. N. (2000). The north sea. *Marine pollution bulletin*, *41*(1-6), 5-23.

Field, C. B. (Ed.). (2014). *Climate change 2014–Impacts, adaptation and vulnerability: Regional aspects*. Cambridge University Press.

Firth, L. B., Thompson, R. C., Bohn, K., Abbiati, M., Airoldi, L., Bouma, T. J., ... & Hawkins, S. J. (2014). Between a rock and a hard place: Environmental and engineering considerations when designing coastal defence structures. *Coastal Engineering*, *87*, 122-135.

Fisher, N., Dolan, R., & Hayden, B. P. (1984). Variations in large scale beach amplitude along the coast. *Journal of Sedimentary Research*, *54*(1), 73-85.

Gijsman, R., Ruessink, B. G., Visscher, J., & Schlurmann, T. (2021). Observations on decadal sandbar behaviour along a large-scale curved shoreline. *Earth Surface Processes and Landforms*, *46*(2), 490-503.

Google Earth Engine (2021). Google Earth Timelapse. Retrieved on: 01-07-2021. Retrieved from: https://earthengine.google.com/timelapse/

Gorelick, N., Hancher, M., Dixon, M., Ilyushchenko, S., Thau, D., & Moore, R. (2017). Google Earth Engine: Planetary-scale geospatial analysis for everyone. *Remote sensing of Environment*, *202*, 18-27.

Grunnet, N. M., & Ruessink, B. G. (2005). Morphodynamic response of nearshore bars to a shoreface nourishment. *Coastal Engineering*, *52*(2), 119-137.

Guillén, J., Stive, M. J. F., & Capobianco, M. (1999). Shoreline evolution of the Holland coast on a decadal scale. *Earth Surface Processes and Landforms: The Journal of the British Geomorphological Research Group*, *24*(6), 517-536.

Haerens, P., Bolle, A., Trouw, K., & Houthuys, R. (2012). Definition of storm thresholds for significant morphological change of the sandy beaches along the Belgian coastline. *Geomorphology*, *143*, 104-117.

Hagenaars, G., de Vries, S., Luijendijk, A. P., de Boer, W. P., & Reniers, A. J. (2018). On the accuracy of automated shoreline detection derived from satellite imagery: A case study of the sand motor mega-scale nourishment. *Coastal Engineering*, *133*, 113-125.

Hardisty, J. (1990). The British Seas: an introduction to the oceanography and resources of the north-west European continental shelf.

Harley, M. D., Turner, I. L., Kinsela, M. A., Middleton, J. H., Mumford, P. J., Splinter, K. D., Phillips, M. S., Simmons, J. A., Hanslow, D. J., & Short, A. D. (2017). Extreme coastal erosion enhanced by anomalous extratropical storm wave direction. *Scientific reports*, *7*(1), 1-9.

Harley, M. D., Turner, I. L., Splinter, K. D., Phillips, M. S., & Simmons, J. A. (2016). Beach response to Australian East Coast Lows: a comparison between the 2007 and 2015 events, Narrabeen-Collaroy Beach. *Journal of Coastal Research*, (75 (10075)), 388-392.

Héquette, A., Hemdane, Y., & Anthony, E. J. (2008). Determination of sediment transport paths in macrotidal shoreface environments: a comparison of grain-size trend analysis with near-bed current measurements. *Journal of Coastal Research*, *24*(3 (243)), 695-707.

Hesp, P. A., & Arens, S. M. (1997). Crescentic dunes at Schiermonnikoog, the Netherlands. *Earth Surface Processes and Landforms: The Journal of the British Geomorphological Group*, *22*(8), 785-788.

Hofstede, J. L. (1999). Process-response analysis for Hörnum tidal inlet in the German sector of the Wadden Sea. *Quaternary International*, *60*(1), 107-117.

Huisman, B. J., Walstra, D. J. R., Radermacher, M., de Schipper, M. A., & Ruessink, B. G. (2019). Observations and modelling of shoreface nourishment behaviour. *Journal of Marine Science and Engineering*, *7*(3), 59.

Kroon, A., & Masselink, G. (2002). Morphodynamics of intertidal bar morphology on a macrotidal beach under low-energy wave conditions, North Lincolnshire, England. *Marine geology*, *190*(3-4), 591-608.

Le Cozannet, G., Oliveros, C., Castelle, B., Garcin, M., Idier, D., Pedreros, R., & Rohmer, J. (2016). Uncertainties in sandy shorelines evolution under the Bruun rule assumption. *Frontiers in Marine Science*, *3*, 49.

Li, N., Yamazaki, Y., Roeber, V., Cheung, K. F., & Chock, G. (2018). Probabilistic mapping of storm-induced coastal inundation for climate change adaptation. *Coastal Engineering*, *133*, 126-141.

Liu, Q., Trinder, J. C., & Turner, I. L. (2017). Automatic super-resolution shoreline change monitoring using Landsat archival data: a case study at Narrabeen–Collaroy Beach, Australia. *Journal of Applied Remote Sensing*, *11*(1), 016036.

Luijendijk, A., Hagenaars, G., Ranasinghe, R., Baart, F., Donchyts, G., & Aarninkhof, S. (2018). The state of the world's beaches. *Scientific reports*, *8*(1), 1-11.

Masselink, G., & Anthony, E. J. (2001). Location and height of intertidal bars on macrotidal ridge and runnel beaches. *Earth Surface Processes and Landforms: The Journal of the British Geomorphological Research Group*, *26*(7), 759-774.

Masselink, G., Castelle, B., Scott, T., Dodet, G., Suanez, S., Jackson, D., & Floc'h, F. (2016). Extreme wave activity during 2013/2014 winter and morphological impacts along the Atlantic coast of Europe. *Geophysical Research Letters*, *43*(5), 2135-2143.

Masselink, G., Hughes, M., & Knight, J. (2014). *Introduction to coastal processes and geomorphology*. Routledge.

Meetnet Vlaamse Banken (2021). Retrieved on: 18-01-2021. Retrieved from: https://meetnetvlaamsebanken.be

Mentaschi, L., Vousdoukas, M. I., Voukouvalas, E., Dosio, A., & Feyen, L. (2017). Global changes of extreme coastal wave energy fluxes triggered by intensified teleconnection patterns. *Geophysical Research Letters*, *44*(5), 2416-2426.

Meteoblue (2020). Retrieved on 16-12-2020. Retrieved from: https://www.meteoblue.com/nl/weer/historyclimate/climatemodelled/schiermonnikoog_nederland_2747591

Miljøminitriet Kystdirektoratet (2021). Retrived on: 29 – 02 – 2021. Retrieved from: https://kyst.dk/soeterritoriet/maalinger-og-data/vandstandsmaalinger/

Morton, R. A. (2002). Factors controlling storm impacts on coastal barriers and beaches: a preliminary basis for near real-time forecasting. *Journal of Coastal Research*, 486-501.

Nienhuis, P. H. (1996). The north sea coasts of Denmark, Germany and the Netherlands. In *Marine Benthic Vegetation* (pp. 187-221). Springer, Berlin, Heidelberg.

Nienhuis, J. H., & van de Wal, R. S. (2021). Projections of global delta land loss from sea-level rise in the 21st century. *Geophysical Research Letters*, e2021GL093368.

NORTH, S. T. F. (1993). *Quality Status Report of the North Sea, Subregion 4*.

Ojeda, E., Ruessink, B. G., & Guillen, J. (2008). Morphodynamic response of a two-barred beach to a shoreface nourishment. *Coastal Engineering*, *55*(12), 1185-1196.

Otsu, N. (1979). A threshold selection method from gray-level histograms. *IEEE transactions on systems, man, and cybernetics*, *9*(1), 62-66.

Pedregosa, F., Varoquaux, G., Gramfort, A., Michel, V., Thirion, B., Grisel, O., Blondel, M., Prettenhofer, P., Weiss, R., Dubourg, V., Vanderplas, J., Passos, A., Cournapeau, D., Brucher, M., Perrot, M., Duchesnay, É. (2011). Scikit-learn:

Machine learning in Python. *the Journal of machine Learning research*, *12*, 2825-2830.

Peuziat, B. (2017). Exploring temporal and spatial variability in sandbar–beach–dune interactions, at Egmond aan Zee, the Netherlands. *MSc Thesis*.

Postma, H. (1982). Hydrography of the Wadden Sea: movements and properties of water and particulate matter. *Ecology of the Wadden Sea*, *1*.

Prakken, A. (1989). Kustlijnvoorspelling Friese Waddeneilanden. *Rijkswaterstaat (Directie Friesland), Rapport ANW-88.44*.

Pranzini, E., & Williams, A. T. (Eds.). (2013). *Coastal erosion and protection in Europe*. Routledge.

Price, T. D., & Ruessink, B. G. (2013). Observations and conceptual modelling of morphological coupling in a double sandbar system. *Earth Surface Processes and Landforms*, *38*(5), 477-489.

Pugh, D. T. (1987). Tides, surges and mean sea level.

Regnauld, H., Jennings, S., Delaney, C., & Lemasson, L. (1996). Holocene sea-level variations and geomorphological response: an example from northern Brittany (France). *Quaternary Science Reviews*, *15*(8-9), 781-787.

Reguero, B. G., Losada, I. J., & Méndez, F. J. (2019). A recent increase in global wave power as a consequence of oceanic warming. *Nature communications*, *10*(1), 1-14.

Ridderinkhof, W., De Swart, H. E., Van der Vegt, M., & Hoekstra, P. (2016a). Modeling the growth and migration of sandy shoals on ebb-tidal deltas. *Journal of Geophysical Research: Earth Surface*, *121*(7), 1351-1372.

Ridderinkhof, W., Hoekstra, P., Van der Vegt, M., & De Swart, H. E. (2016b). Cyclic behavior of sandy shoals on the ebb-tidal deltas of the Wadden Sea. *Continental Shelf Research*, *115*, 14-26.

Rijkswaterstaat (2021a). Retrieved on: 18-01-2021. Retrieved from: https://waterinfo.rws.nl/#!/kaart/Waterhoogten/Waterhoogte___20berekend___20Oppervlaktewater___20t.o.v.___20Normaal___20Amsterdams___20Peil___20in___20cm,Waterhoogte___20Oppervlaktewater___20t.o.v.___20Normaal___20Amsterdams___20Peil___20in___20cm/

Rijkswaterstaat (2021b). Retrieved on: 11–05–2021. Retrieved from: https://waterberichtgeving.rws.nl/water-en-weer/verwachtingen-water/water-en-weerverwachtingen-waternoordzee/stormvloedrapportages/stormvloedverslagen

Ruessink, B. G., Coco, G., Ranasinghe, R., & Turner, I. L. (2007). Coupled and noncoupled behavior of three-dimensional morphological patterns in a double sandbar system. *Journal of Geophysical Research: Oceans*, *112*(C7).

Ruessink, B. G., & Jeuken, M. C. J. L. (2002). Dunefoot dynamics along the Dutch coast. *Earth Surface Processes and Landforms: The Journal of the British Geomorphological Research Group*, *27*(10), 1043-1056.

Ruessink, B. G., Pape, L., & Turner, I. L. (2009). Daily to interannual cross-shore sandbar migration: Observations from a multiple sandbar system. *Continental Shelf Research*, *29*(14), 1663-1677.

Ruessink, G., Schwarz, C. S., Price, T. D., & Donker, J. J. (2019). A Multi-Year Data Set of Beach-Foredune Topography and Environmental Forcing Conditions at Egmond aan Zee, The Netherlands. *Data*, *4*(2), 73.

Rutten, J., Dubarbier, B., Price, T. D., Ruessink, B. G., & Castelle, B. (2019). Alongshore variability in crescentic sandbar patterns at a strongly curved coast. *Journal of Geophysical Research: Earth Surface*, *124*(12), 2877-2898.

Rutten, J., Ruessink, B. G., & Price, T. D. (2018). Observations on sandbar behaviour along a man-made curved coast. *Earth Surface Processes and Landforms*, *43*(1), 134-149.

Scott, T., Masselink, G., O'Hare, T., Saulter, A., Poate, T., Russell, P., ... & Conley, D. (2016). The extreme 2013/2014 winter storms: Beach recovery along the southwest coast of England. *Marine Geology*, *382*, 224-241.

Sha, L. P. (1989a). Sand transport patterns in the ebb-tidal delta off Texel Inlet, Wadden Sea, The Netherlands. *Marine Geology*, *86*(2-3), 137-154.

Sha, L. P. (1989b). Variation in ebb-delta morphologies along the West and East Frisian Islands, The Netherlands and Germany. *Marine Geology*, *89*(1-2), 11-28.

Short, A. D. (1991). Macro-meso tidal beach morphodynamics: an overview. *Journal of Coastal Research*, 417-436.

Small, C., & Nicholls, R. J. (2003). A global analysis of human settlement in coastal zones. *Journal of coastal research*, 584-599.

Splinter, K. D., Turner, I. L., Davidson, M. A., Barnard, P., Castelle, B., & Oltman-Shay, J. (2014). A generalized equilibrium model for predicting daily to interannual shoreline response. *Journal of Geophysical Research: Earth Surface*, *119*(9), 1936-1958.

Stive, M. J., Aarninkhof, S. G., Hamm, L., Hanson, H., Larson, M., Wijnberg, K. M., ... & Capobianco, M. (2002). Variability of shore and shoreline evolution. *Coastal engineering*, *47*(2), 211-235.

Stronkhorst, J., Huisman, B., Giardino, A., Santinelli, G., & Santos, F. D. (2018). Sand nourishment strategies to mitigate coastal erosion and sea level rise at the coasts of Holland (The Netherlands) and Aveiro (Portugal) in the 21st century. *Ocean & Coastal Management*, *156*, 266-276.

USGS (2021). Retrieved on 27-05-2021. Retrieved from: https://www.usgs.gov/core-science-systems/nli/landsat/landsat-7?qt-science_support_page_related_con=0#qt-science_support_page_related_con

Van de Lageweg, W. I., Bryan, K. R., Coco, G., & Ruessink, B. G. (2013). Observations of shoreline–sandbar coupling on an embayed beach. *Marine Geology*, *344*, 101-114.

Van de Meene, J. W., & van Rijn, L. C. (2000). The shoreface-connected ridges along the central Dutch coast—part 1: field observations. *Continental Shelf Research*, *20*(17), 2295-2323.

Van der Walt, S., Scho€nberger, J.L., Nunez-Iglesias, J., Boulogne, F., Warner, J.D., Yager, N., Gouillart, E., Yu, T. (2014). scikit-image: image processing in Python. *PeerJ*, *2*, e453.

Van Duin, M. J. P., Wiersma, N. R., Walstra, D. J. R., Van Rijn, L. C., & Stive, M. J. F. (2004). Nourishing the shoreface: observations and hindcasting of the Egmond case, The Netherlands. *Coastal Engineering*, *51*(8-9), 813-837.

Van Houwelingen, S., Masselink, G., & Bullard, J. (2006). Characteristics and dynamics of multiple intertidal bars, north Lincolnshire, England. *Earth Surface Processes and Landforms: The Journal of the British Geomorphological Research Group*, *31*(4), 428-443.

Van Lancker, V. R. M. (2001). Sediment and morphodynamics of a siliciclastic near coastal area, in relation to hydrodynamical and meteorological conditions: Belgian Continental Shelf= De sediment-en morfodynamiek van de kustnabije zone in relatie tot de impact van hydrodynamische en meteorologische factoren in een silicoclastische omgeving, Belgisch continentaal plat. *Unpublished.*

Van Oyen, T., Van Lancker, V., & de Swart, H. (2013). De Noordzeebodem: een landschap vol pieken en dalen. *De Grote Rede*, *35*, 17-22.

Van Rijn, L. C., Ruessink, B. G., & Mulder, J. P. M. (Eds.). (2002). *Coast3D-Egmond: The Behaviour of a Straight Sandy Coast on the Time Scale of Storms and Seasons: Process Knowledge and Guidelines for Coastal Management: End Document, March 2002*. Aqua Publications.

Vanagt, T., Van de Moortel, L., Heusinkveld, J., Eede, S. V., & Van Steenbrugge, L. (2011). Veldcampagne ecologie Ameland 2010.

Vos, K., Harley, M. D., Splinter, K. D., Simmons, J. A., & Turner, I. L. (2019a). Sub-annual to multi-decadal shoreline variability from publicly available satellite imagery. *Coastal Engineering*, *150*, 160-174.

Vos, K., Splinter, K. D., Harley, M. D., Simmons, J. A., & Turner, I. L. (2019b). CoastSat: A Google Earth Engine-enabled Python toolkit to extract shorelines from publicly available satellite imagery. *Environmental Modelling & Software*, *122*, 104528.

Wang, Z. B., Hoekstra, P., Burchard, H., Ridderinkhof, H., De Swart, H. E., & Stive, M. J. F. (2012). Morphodynamics of the Wadden Sea and its barrier island system. *Ocean & coastal management*, *68*, 39-57.

Wijnberg, K. M. (2002). Environmental controls on decadal morphologic behaviour of the Holland coast. *Marine Geology*, *189*(3-4), 227-247.

Winkelmolen, A. M., & Veenstra, H. J. (1980). The effect of a storm surge on near-shore sediments in the Ameland-Schiermonnikoog area (N. Netherlands). *Geologie & mijnbouw*, *59*(2), 97-111.

Winter, G. (2012). Rip Current Characteristics at the Dutch Coast: Egmond aan Zee.

Xu, H. (2006). Modification of normalised difference water index (NDWI) to enhance open water features in remotely sensed imagery. International journal of remote sensing, 27(14), 3025-3033.

Yates, M. L., Guza, R. T., & O'reilly, W. C. (2009). Equilibrium shoreline response: Observations and modeling. *Journal of Geophysical Research: Oceans*, *114*(C9).

Young, I. R., & Ribal, A. (2019). Multiplatform evaluation of global trends in wind speed and wave height. *Science*, *364*(6440), 548-552.